A Fundamental Study of the Morphological Acceleration Factor

Liang Li

August 30, 2010

A fundamental study of the Morphological Acceleration Factor

Liang Li

Graduation committee:

Prof. dr. ir. M.J.F Stive	Delft University of Technology, Chairman
Dr. M.J.A. Borsboom	Deltares
Dr. ir. R. J. Labeur	Delft University of Technology
Dr. W.M.R.J.B.Ranasinghe	Delft University of Technology / UNESCO-IHE
Ir. C.M.Swinkels	Deltares
Ir. D.J.R.Walstra	Delft University of Technology / Deltares

Contents

Preface

Research is what I'm doing when I don't know what I'm doing.

Wernher Von Braun[1]

This Master Thesis is written as a final part of my master study at Hydraulic Engineering at the Faculty of Civil Engineering at Delft University of Technology.

This report is an overview of a fundamental study on the morphological acceleration factor using eigenvalue analysis. The main research objective is to obtain a proper insight into the effect and the determining factors of Morfac. An upper limit of Morfac based on the stability and accuracy analysis is derived.

This study is held by the Harbor, Coastal and Offshore Engineering Department of Deltares. I am grateful to the members of the graduation commission for their supervision and dedication. First, I would like to thank Marcel Stive for being the chairman of the committee. Rosh Ranasinghe

[1] A German-American rocket scientist, astronautics engineer and space architect from the National Aeronautics and Space Administration (NASA)

and Dirkjan Walstra offered me this opportunity and Cilia Swinkels for her guidance at Deltares. I would further like to thank Mart Borsboom and Robert Jan Labeur for their help in mathematics.
Finally, I am, of course, particularly indebted to my parents and my girlfriend Peipei for their unwavering support and encouragement on all fronts.

Liang Li
Delft, August 2010

Abstract

Long-term prediction of sediment transport and morphology has become increasingly important. One of the key issues in carrying out long-term modeling is to bridge the gap between short-term hydrodynamics varying from hours to days, and morphological changes, taking place over much longer periods.

Lesser et al. (2004) and Roelvink (2006) have introduced the powerful concept of the morphological acceleration factor (Morfac) to coastal morphodynamic modeling, which potentially enables modelers to simulate morphological evolution in coastal areas at the time scales of decades.

In this thesis, the effects and limits of the concept of Morfac in coastal morphodynamic modeling are studied from a 1D analytical model with unidirectional flow, and the model with numerical implementation. After linearized and non-dimensionalized, the sensitivity of the Morfac is analyzed based on investigating Froude number, sediment transport factor ψ, friction parameter, Courant number and points per wavelength. The criteria of the Morfac is derived both from stability and accuracy. In Chapter 5, an 1D Delft3D model is performed to reproduce and prove the conclusions from the analysis results in Chapter 3 and 4.

Forcing parameters such as the flow velocity magnitude is the dominant

factor while the model properties like the grid size and time step play a minor role. A necessary stability criteria is derived for this specific 1D case, $MF \times \psi \times Cr^{0.6} \leq 0.63$. In the analytical and numerical models, Morfac performs better than in the Delft3D model. A strong recommendation is to further improve the numerical implementation of Delft3D which may extensively increase the value of Morfac we can use. For the accuracy analysis in this Delft3D model, benchmark is taken as Morfac equals to one. If bed level amplitude change after one wavelength is focused, a Morfac that satisfies the relation $MF \times \psi \geq 10^{-3}$ will usually cause more than 1% of error.

List of Figures

List of Tables

Chapter 1

Introduction

1.1 Background

Long-term prediction of morphological evolution of estuaries, or the coastal zones in response to climate change, human interference or a changing local environment, is an increasingly important issue for the threats of accelerated sea-level rise and need for sustainable development. Not only the bed topography but also the ecosystem is important in longterm evolution (sediment quality, pollutants, nutrients adhering to the sediment) (de Vriend et al. [4]).

Because our knowledge is still insufficient on which short-term processes are important in the long run, although some existing coastline models cover significant time scales, they do not give dynamic evolution which may oversimplify the real nature. Process-based numerical model solving mathematical formulations able to give more intrinsic properties and forcing process rather than the empirical relations (See details in de Vriend [3]. Coastal behavior is the result of a large number of processes and mechanisms which act and interact on a variety of spatial and temporal scales. (See Figure (1.1)) Running a real-time model which reproduce the short-term processes and run on a long-term leads to prohibitively time consuming computation. Several

techniques are applied to accelerate the computations, like input reduction, model reduction and behavior-oriented modeling which are discussed in de Vriend et al. [4]. In practice, usually a combination of these techniques is used. The same key idea behind these techniques is to fill in the gap between short-term hydrodynamic behavior and long-term morphological changes.

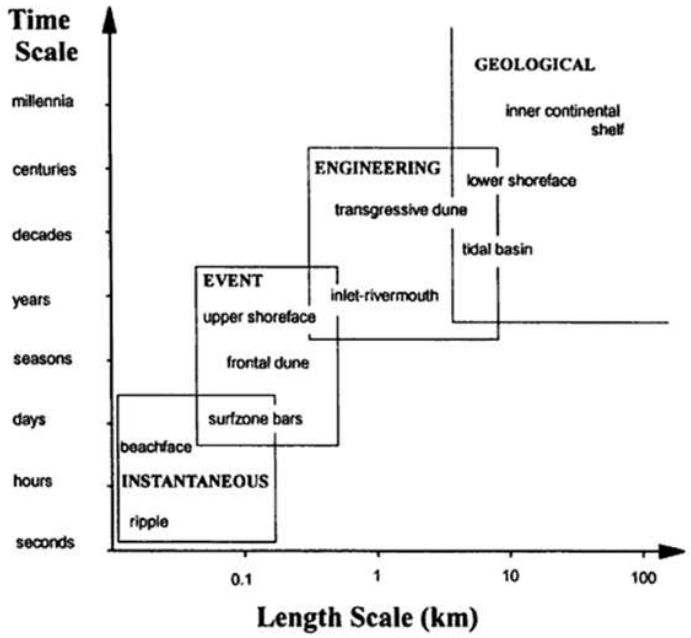

Figure 1.1: *Spatial and temporal scales of coastal processes (after Cowell and Thom [2])*

1.2 Long-term morphology updating techniques in model reduction

One of the complications inherent in carrying out morphological computational predictions on the basis of hydrodynamic flows is that morphological developments take place on a time scale several times longer than typical flow changes. Wang et al.[12] prove that hydrodynamic behavior in estuaries has a time scale that is typically 1 to 2 orders of magnitude smaller than

the morphodynamic time scale. In terms of numerical modeling this implies that many hydrodynamic calculations need to be performed which is the most expensive in terms of computational times but have only limited effect on the morphology. It is only after several weeks that the impact on the bed becomes relevant. Morphodynamic calculations would therefore require long and inefficient hydrodynamic calculation time. In order to increase the efficiency of process-based morphodynamic models, different upscaling techniques have been developed.

In the historical processes, the four techniques stated below is the most popular used and will be discussed in detail in Chapter 2. The classical 'tide-averaging' approach, in combination with the 'continuity correction' and the 'RAM' approach (Rapid Assessment of Morphology) are old offline techniques, in which the morphodynamics are updated less frequently than the hydrodynamics. The 'morphological acceleration factor (or Morfac)' and 'parallel online' approach are most advanced online techniques which the transport field and bottom changes are computed instantaneous after each hydrodynamic step [9].

1.3 Morfac approach and basic concept

'Morphological acceleration factor (Morfac)' is an approach whereby the speed of the changes in the morphology is scaled up to a rate that it not yet begins to have a significant impact on the hydrodynamic flows. The implementation of Morfac is achieved by simply multiplying the bed level changes by a non-unity factor (Morfac) after each hydrodynamic time step which enables the computation of sediment transport and morphological change simultaneously with the hydrodynamics. This simplifies the model setup and operation in comparison with other approaches. The Morfac can also be applied in a fully three-dimensional flow and sediment transport

computation.

Delft3D, the model used in this study is a processed-based numerical morphological model where the flow fields are solved first and stored for the sediment transport module. In the recent version of Delft3D, an online Morfac approach is implemented, which couples the hydrodynamic, sediment transport, and morphology change.

The main advantage of the application of Morfac is (more details in Lesser [6]):

1. The computational time is significantly reduced compared to full morphological model without acceleration.

2. The feedback from the morphology is immediately brought to hydrodynamic calculations.

3. Sediment transport and morphology calculation is simple to perform.

Despite all the advantages of the Morfac, the application of the Morfac also brings some drawbacks.

For bedload transport, the Morfac multiplies the bedload transport rates. For suspended load transport, the Morfac multiplies the exchange of sediment (erosive or depositional flux) at the bed-water interface. When there is sufficient sediment on the bed, the magnitude of sediment concentrations in the water column is not modified just the exchange rate with the bed. When the availability of sediment is limited, the Morfac will change the concentration in order to keep the transport equation mass conservative. Consequently, the concentration in these areas are artificially low, which is not suitable for locations where sediment stratification is a big issue.

The Morfac upscales the bed dynamics by a constant factor, but in reality, there exists both vertical growing and horizontal propagation. Intuitively, if Morfac does not upscaled both direction at the same rate, there will be

a Morfac induced error. See Figure (1.2) for sketch of illustrating a phase error .

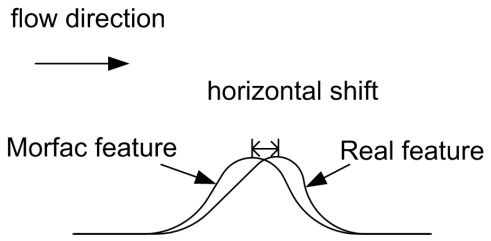

Figure 1.2: *Horizontal phase shift by Morfac*

The application of the Morfac is a numerical trick to allow fast computations, though it introduces errors. As long as the error is acceptable, it is worthwhile to apply a Morfac.

Lots of morphodynamic modeling studies using the Delft3D online Morfac approach have been published.

Grunnet el al.[5] used a Morfac around 10 for simulation of morphological change after a beach nourishment during 5 months. Reniers el al. [8] examined the morphodynamic response of nearshore zone of an embayed beach induced by wave groups. In his model, a Morfac of 8 is used. Most recently, van der Wegen [11] applied a Morfac of 400 to investigate the evolution of a schematized tidal basin over several centuries.

Although the Morfac approach has proven its practical applicability in several studies, but all the values of Morfac are heuristically determined. The present study aims to address this knowledge gap and its strength and limitations.

1.4 Aims and objective

The main aim of the thesis is to study the fundamental effect of Morfac to the accuracy of the model and to derive a criteria for specifying Morfac in some specific cases.

Not only the effect of the local environment is investigated but also the reason for the effect. In order to avoid the complexity of the model, a 1D model is studied, and the flow is unidirectional. The sensitivity and deterministic of Morfac will be studied. The objectives state as follows:

1. Study the error induced by Morfac and what kind of unrealistic physical behavior it induced.

2. Study the combination of Morfac induced errors and other numerical errors.

3. Derive a criteria for an the prior determination of the upper limit of Morfac.

1.5 Thesis outline

To meet the objections, the thesis is organized as follows. Chapter 2 presents a summary of available upscaling techniques and previous conclusions on Morfac.
In Chapter 3, a simplified analytical model is studied including friction and non-friction case. The effect of Morfac to the celerity and amplitude as a function of Froude number, sediment transport factor, Morfac and the friction are studied.
In Chapter 4, the analytical model is discretized by the numerical scheme presently implemented in Delft3D. Besides the elements studied in the analytical model, Courant number and points per wavelength are included.
In Chapter 5, several test runs are performed in Delft3D to validate the conclusions from the previous Chapters.
Conclusions and recommendations for further work is given in Chapter 6.

Chapter 2

Morphology updating techniques

The computational time of a process-based numerical morphological model is intensive and strongly depends on the resolution, involved processes, and computational capability. Normally the simulation time is at a speed in the order of just 10 times faster than real time. If a longterm morphological evolution of years or even decades is studied, morphological acceleration techniques are required.
In de Vriend et al. [4], three distinct approaches of morphological acceleration techniques are stated.

1. Input reduction: The longterm residual effect of smaller-scale processes can be obtained by forcing these models with 'representative' inputs.

2. Model reduction: The scale of interest in reformulated without describing the details of the smaller-scale processes.

3. Behavior-oriented reduction: The phenomenon of interest is modeled without describing underlying processes.

In this chapter, only the strategies of morphological updating in model reduction is investigated. However, in order to effectively use the model re-

duction technique, it is also necessary to apply input reduction. Because the time scale of the forcing processes are now decoupling with morphology.

2.1 Tide-averaging and continuity correction

The classic tide-averaging approach assumes the morphological changes in a single tidal cycle or even several tidal cycles are small compared to the long-term trend. Then it is reasonable to keep a fixed bottom when computing hydrodynamics and sediment transport over a tidal cycle. The averaged sediment transport result is applied to compute bed changes. Then modified bathymetry is fed back to the transport field through continuity correction. The sediment transport field is usually a function of flow velocity and orbital velocity. If the flow pattern is assumed not to vary with small bed changes, then adaptation of transport field is only a matter of adjusting the flow and orbital velocity. A number of velocities based on the original water depth are stored and when water depth changes, the transport is calculated on the adapted depth at several time points in a tidal cycle. After an entire tidal cycle, a full transport computation is needed.

Figure (2.1) shows the flow diagram of tidal-averaging approach combined with continuity correction. In shallow area, the velocities will keep increasing by continuity correction, which becomes a main limitation for the continuity correction assumption, for a shallow area, friction will become important.

2.2 RAM approach

Initial sedimentation/erosion rates are usually used in consultancy projects which the outcome of initial transport computations need to be interpreted without having to resort to full morphodynamic simulations, i.e. models using the bottom topography as an input parameter into the hydrodynamic and sediment-transport consituents. The method is not able to give correct

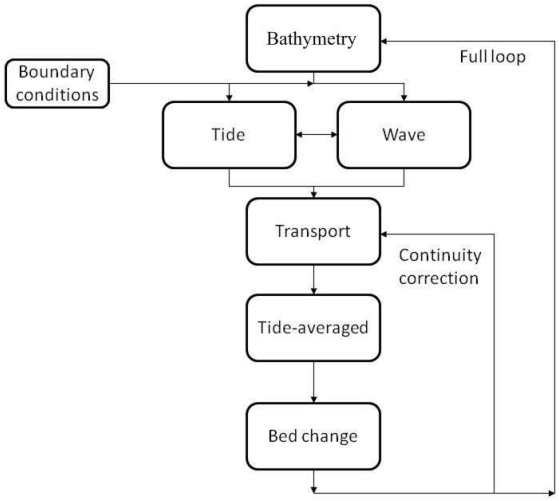

Figure 2.1: *Flow diagram of tidal-averaging and continuity correction (Modified from Roelvink [9])*

relation between the direction of migration and transport. The RAM (Rapid Assessment of Morphology) module in Delft3D is a simple method which overcomes the disadvantage. In the RAM approach, flow and wave patterns are assumed to be invariant for small bottom changes. So the transport field is only a function of water depth and solved in a simple relation. An important point in RAM approach is that the costly hydrodynamics computations can be carried out in parallel, using different processors. The flow diagram is shown in Figure (2.2). RAM quick updating scheme is suitable for long time and large spatial scales when a lot of conditions are involved.

2.3 Online approach with Morfac

Lesser et al. [7] introduced a powerful concept of the morphological acceleration factor (Morfac) to coastal morphodynamic modeling, which exploits the elegant 'online' approach which runs the flow, sediment transport and bottom are all updated at the same time.

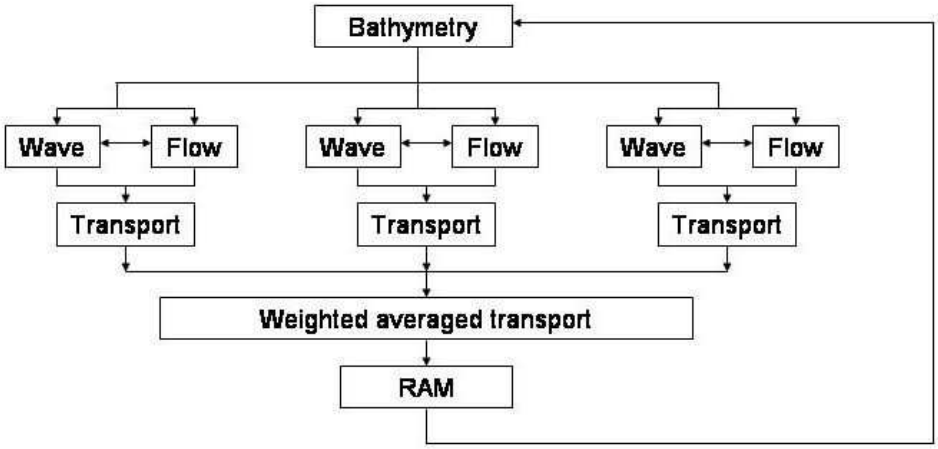

Figure 2.2: *Flow diagram of RAM approach (Modified from Roelvink [9])*

The morfac concept (implemented in Delft3D) essentially multiplies the bed levels computed after each hydrodynamic time step by a constant factor to enable faster computation. The significantly upscaled new bathymetry is then used in the next hydrodynamic step. See the flow diagram of the Morfac approach in Figure (2.3).

The important difference with the 'tide-averaging' and 'RAM' method is the bottom evolution is computed in much smaller time steps. Consequently, the short-term processes are coupled at flow time-step level. The various interactions between flow, sediment and morphology is easy to included.

2.4 Parallel online approach

This new method is like the online RAM approach, it assumes that hydrodynamic conditions vary much more rapidly than the morphology can follow. This is allowed if the time interval within which all different conditions (ebb, flood, slack, spring tide, neap tide, NW storm, SW wind, etc.) may occur is small relative to the morphological time scale. So all the simulations for dif-

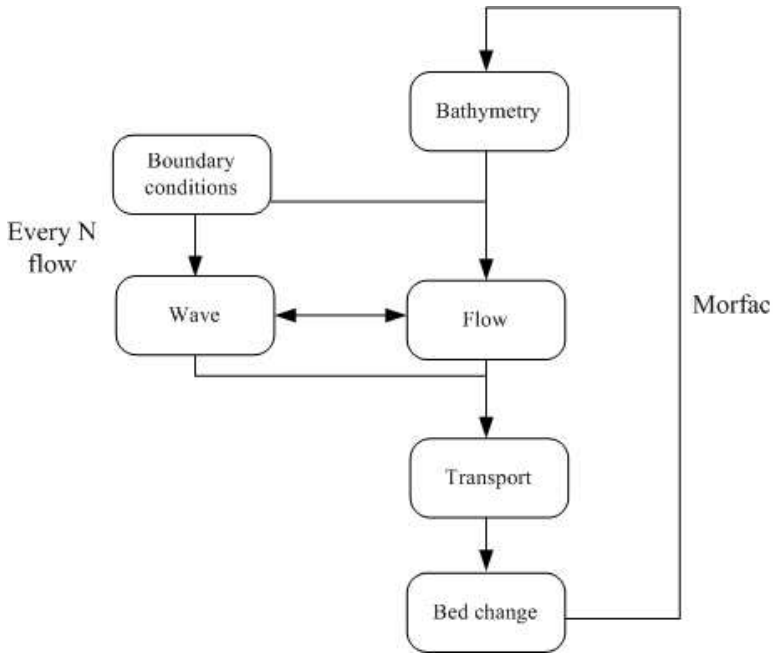

Figure 2.3: *Flow diagram of Morfac approach*

ferent conditions can run in parallel and share the same bathymetry which is updated according to the weighted average of bottom changes due to each condition. See Figure (2.4) for the flow diagram. The simulation is split into several parallel processes, makes an efficient implementation of computers. Roelvink [9] gives a more complete overview of available upscaling methods. It was also proved that the online approach gives more accurate results than offline approach. Online Morfac approach now is the standard in Delft3D-MOR module. Several previous studies have been made to derive criteria for applying Morfac.

2.5 Historical research on Morfac

Approach

In order to test the sensitivity and dependency of Morfac which is implemented in Delft3D to forcing and model parameters, the way it has been

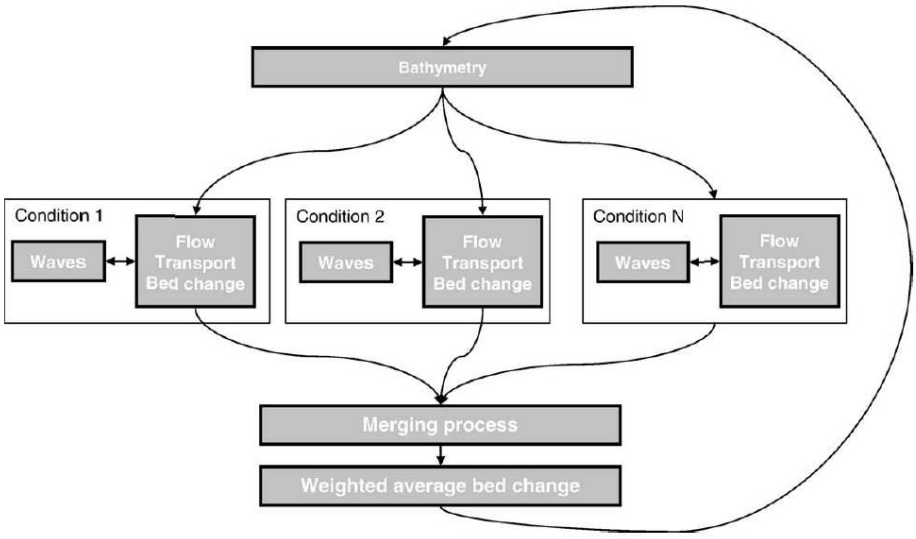

Figure 2.4: *Flow diagram of parallel online approach (Roelvink [9])*

analyzed before has been based on runs with the Delft3D model. The most accurate numerical model simulation currently possible is one undertaken with Morfac equals to one. In other words, the morphology development is not accelerated. The model predictions with various higher Morfac can be tested against this benchmark case.

This is a straightforward approach to study Morfac. By comparing the end result for each simulation with the benchmark, the development of errors can be determined for increasing Morfac.

The root mean square error (RMSE) and the Brier skill scores (BSS) are used to quantify the errors introduced into the model. The RMSE is a domain-specific measurement, which only shows the error for s single case.

$$BSS = 1 - \frac{\langle (z_b - z_{b,mf1})^2 \rangle}{\langle (z_1 - z_{b,mf1})^2 \rangle} \tag{2.1}$$

where z_b is the final bed level, z_1 is the initial bed level, and $z_{b,mf1}$ is the final bed level for the reference case (Morfac equals to one).

BSS is defined by Equation (2.1) though is not domain specific, it does not help provide qualitative information how, why, when or where a model result

deviates from the beach mark case.
Several test runs with different simple geometry in 1D and 2D model have been done by C.M. Swinkels [1], and the results show:

1. The higher the Morfac, the more divergence it is from the benchmark case.

2. The model error for higher Morfac with respect to Morfac equal to one is time dependent and grows with time.

3. The effect of Morfac to suspended transport and bed load transport is different.

4. Flow velocity has a dominant effect on the maximum applicable Morfac. Grid resolution and time step also play an important role.

Several questions still remains:

1. What is the effect of Morfac on hydrodynamics?

2. What is the exact effect of Morfac in the model despite the complex numerical model properties?

3. What is the numerical effects?

2.6 Fundamental research approach on Morfac

In order to remove all the unknown and non-transparent effects in Delft3D and to investigate the control parameter of Morfac, a fundamental research approach is developed. The governing equations in Delft3D are studied directly at the first stage, we call it the analytical model. In the analytical model, the error could only be the Morfac error. Then a certain numerical scheme is used for the analytical model, now in the system, there are two contributions, one is the Morfac, the other is the numerical scheme. Finally,

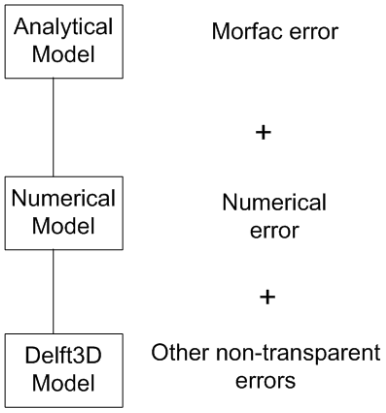

Figure 2.5: *Fundamental research*

Delft3D model is studied again, which is the most complex, but based on the preliminary results from the analytical model and numerical model, it is easy to isolate the effect of Morfac from the others.

Eigenvalue analysis

The governing equations are non-linear partial differential equations, but can be linearized, and the resulting linearized equations can be used to investigate the system's response to small variations in the input or state variables, starting at an equilibrium point.

So what we do is we assume an initially equilibrium situation, and expose a small perturbation into the system. To every mode, we plugged in, there is a set of eigenvalues for the existing non-trivial solutions. And the eigenvalues give the propagation information of this perturbation which we are interested in. Mainly, the deviation of eigenvalues with and without Morfac is the error which Morfac brings into the model.

The eigenvalues of a linearized set of equations are calculated. But in practice, there is only non-linear systems, the eigenvalues depend on the system state and they change when the system state evolves. Therefore, a set of eigenvalues only characterizes the actual state of the system and not necessarily other states.[10]

Chapter 3

Analysis of Morfac in analytical model

The fundamental effect of Morfac in Delft3D-FLOW module is going to be investigated. It solves the unsteady shallow water equations in two (depth-averaged) or three dimensions. Because Delft3D-FLOW module itself is a complex model and already includes some untransparent numerical effects, which makes it difficult to analyze from the model itself. Therefore, the group of equations which Delft3D-FLOW solves will be studied. And in order to further simplify the analysis, the 1D shallow water equations are used here. The equations consist of the momentum equation, the continuity equation, and the sediment transport equation including morphology update. Through this analysis, the basic behavior of Morfac and the determined parameters will be derived from this system.

3.1 Model description

Figure 3.1 is a sketch of the 1D analytical model. Where U is the velocity; z_b is the bed level; ζ is the water level. The reference level in the 1D model is the mean water level and the positive direction is defined upwards, thus

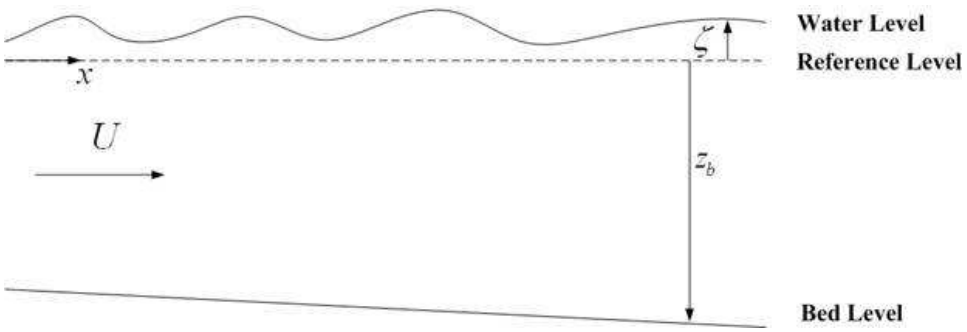

Figure 3.1: *Sketch of 1D analytical model*

the total water depth h is now defined as $h = \zeta - z_b$, in which z_b is negative. Some assumptions are made to make the analytical model easy to analyze.

1. A unidirectional flow is assumed in the domain and in the positive x direction.

2. Friction term is written as $gU^2/(C^2h)$, where C is the Chézy friction coefficient and assumed to be depth independent.

3. The sediment transport is assumed to be a function of local velocity $S = f(U)$, which is a form of bed-load transport equation.

4. Morfac is the morphological acceleration factor, which directly multiplies the sediment transport, when bed load is assumed.

The simplified 1D shallow water equations are:

- Momentum equation

$$\frac{\partial U}{\partial t} + U\frac{\partial U}{\partial x} + g\frac{\partial \zeta}{\partial x} = -g\frac{U^2}{C^2 h} \tag{3.1}$$

- Continuity equation

$$\frac{\partial \zeta}{\partial t} + \frac{\partial hU}{\partial x} = 0 \tag{3.2}$$

- Sediment transport

$$\frac{1}{MF}\frac{\partial z_b}{\partial t} + \frac{\partial S}{\partial x} = 0 \tag{3.3}$$

3.2 Linearized and dimensionless equations

Perturbation analysis

The system of equations is a non-linear system consisting of three nonlinear terms: the friction term, the advection term and the sediment transport term. In order to find analytical solutions, it is possible to linearize the system by studying the variation from an originally equilibrium situation (perturbation analysis):

$$U = U_0 + U^{'}$$

$$\zeta = \zeta_0 + \zeta^{'}$$

$$z_b = z_{b,0} + z_b^{'} \tag{3.4}$$

where the subscript 0 represents original equilibrium situation, and the superscript is the small perturbation. The non-linear terms containing perturbations are not leading order.

1. Advection term: take $U\partial U/\partial x$ term as an example

$$U\frac{\partial U}{\partial x} = (U_0 + U^{'})\frac{\partial (U_0 + U^{'})}{\partial x} = U_0\frac{\partial U_0}{\partial x} + U_0\frac{\partial U^{'}}{\partial x} + U^{'}\frac{\partial U_0}{\partial x} + U^{'}\frac{\partial U^{'}}{\partial x}$$

According to the equilibrium assumptions, the equilibrium velocity is slowly varying, which means that $\partial U_0/\partial x$ is smaller than or in the same order as $\partial U^{'}/\partial x$. Thus

$$|U^{'}\frac{\partial U_0}{\partial x}| \ll |U_0\frac{\partial U^{'}}{\partial x}|$$

$U'\partial U_0/\partial x$ can be neglected. And $U^{'}\partial U^{'}/\partial x$ is a second order of the small perturbation which can also be neglected. Consequently

$$U\frac{\partial U}{\partial x} \approx U_0\frac{\partial U_0}{\partial x} + U_0\frac{\partial U^{'}}{\partial x}$$

2. The transport derivative is a highly nonlinear term with the approximated relationship of $S = f(U)$,

$$\frac{dS}{dx} = \frac{dS}{dU} \cdot \frac{dU}{dx} = f_U(U_0 + U')\frac{dU}{dx} \approx f_U(U_0)\frac{dU}{dx}$$

Where $f_U = df(U)/dU$

3. The friction term is also a nonlinear term in the flow velocity

$$-g\frac{(U_0 + U^{'})^2}{C^2(h_0 + h')} = -g\frac{U_0^2 + U^{'2} + 2U_0U^{'}}{C^2(h_0 + h')}$$

where $U^{'2}$ is the second order of small perturbation, which can be neglected and

$$\frac{1}{h_0 + h^{'}} = \frac{1}{h_0}\frac{1}{1 + \frac{h'}{h_0}} = \frac{1}{h_0}(1 - \frac{h^{'}}{h_0} + \mathrm{O}(h^{'2}))$$

is the Taylor series expansion. Thus

$$-g\frac{(U_0 + U^{'})^2}{C^2(h_0 + h')} \approx -g\frac{U_0^2 + 2U_0U^{'}}{C^2h_0}(1 - \frac{h^{'}}{h_0}) \approx -g\frac{U_0^2}{C^2h_0} + g\frac{U_0^2h^{'}}{C^2h_0^2} - g\frac{2U_0U^{'}}{C^2h_0}$$

The background solution satisfies:

$$\frac{\partial U_0}{\partial t} + U_0\frac{\partial U_0}{\partial x} + g\frac{\partial \zeta_0}{\partial x} + g\frac{U_0^2}{C^2h_0} = 0$$

$$\frac{\partial \zeta_0}{\partial t} + \frac{\partial h_0U_0}{\partial x} = 0$$

$$\frac{1}{MF}\frac{\partial z_{b,0}}{\partial t} + f_U(U_0)\frac{\partial U_0}{\partial x} = 0$$

The linearized momentum equation for the perturbations if the background solutions are neglected is:

$$\begin{aligned}&\frac{\partial U_0}{\partial t} + \frac{\partial U^{'}}{\partial t} + U_0\frac{\partial U_0}{\partial x} + U_0\frac{\partial U^{'}}{\partial x} + g\frac{\partial \zeta_0}{\partial x} + g\frac{\partial \zeta^{'}}{\partial x} + g\frac{U_0^2}{C^2h_0} - g\frac{U_0^2h^{'}}{C^2h_0^2} + g\frac{2U_0U^{'}}{C^2h_0}\\ &= \frac{\partial U^{'}}{\partial t} + U_0\frac{\partial U^{'}}{\partial x} + g\frac{\partial \zeta^{'}}{\partial x} - g\frac{U_0^2h^{'}}{C^2h_0^2} + g\frac{2U_0U^{'}}{C^2h_0}\end{aligned} \tag{3.5}$$

The same for the continuity and sediment transport equation:

$$\frac{\partial \zeta'}{\partial t} + h_0\frac{\partial U'}{\partial x} + U_0\frac{\partial \zeta'}{\partial x} - U_0\frac{\partial z_b'}{\partial x} = 0 \tag{3.6}$$

$$\frac{\partial z_b'}{\partial t} + MF \times f_U(U_0)\frac{\partial U'}{\partial x} = 0 \tag{3.7}$$

Substitute into the governing equations and in a matrix form:

$$\begin{aligned}\frac{\partial}{\partial t}\begin{pmatrix} U' \\ \zeta' \\ z_b' \end{pmatrix} + \begin{pmatrix} U_0 & g & 0 \\ h_0 & U_0 & -U_0 \\ MF \times f_U(U_0) & 0 & 0 \end{pmatrix}\frac{\partial}{\partial x}\begin{pmatrix} U' \\ \zeta' \\ z_b' \end{pmatrix} \\ + \begin{pmatrix} 2gU_0/C^2h_0 & -gU_0^2/C^2h_0^2 & gU_0^2/C^2h_0^2 \\ 0 & 0 & 0 \\ 0 & 0 & 0 \end{pmatrix}\begin{pmatrix} U' \\ \zeta' \\ z_b' \end{pmatrix} = 0\end{aligned} \tag{3.8}$$

It can also be written as:

$$\frac{\partial \phi}{\partial t} + A\frac{\partial \phi}{\partial x} + B\phi = 0 \tag{3.9}$$

Where:

$$\phi = \begin{pmatrix} U' \\ \zeta' \\ z_b{}' \end{pmatrix}$$

$$A = \begin{pmatrix} U_0 & g & 0 \\ h_0 & U_0 & \text{-}U_0 \\ MF \times f_U & 0 & 0 \end{pmatrix}$$

$$B = \begin{pmatrix} 2gU_0/C^2h_0 & \text{-}gU_0{}^2/C^2h_0{}^2 & gU_0{}^2/C^2h_0^2 \\ 0 & 0 & 0 \\ 0 & 0 & 0 \end{pmatrix}$$

Dimensionless equations

Dimensionless systems give better insight in the relative importance of different factors. A typical horizontal length scale for the perturbation λ_T, vertical depth scale h_0, velocity scale c_T, and time scale T_T for the

corresponding λ_T are introduced to further dimensionless the equations. To these scales, the following relations hold:

$$c_T = \sqrt{gh_0}$$

$$\lambda_T = c_T T_T \tag{3.10}$$

So now every variable can be written as a dimensionless value times a typical scale.

$$\begin{aligned} U^{'} &= U_D c_T \\ \zeta^{'} &= \zeta_D{}^{'} h_0 \\ z_b^{\prime} &= z_{b,D}{}^{'} h_0 \\ x &= x_D \lambda_T = x_D c_T T_T \\ t &= t_D T_T \end{aligned}$$

Consequently, the dimensionless equations are

$$\frac{\partial}{\partial t_D}\begin{pmatrix} U_D \\ \zeta_D \\ z_{b,D} \end{pmatrix} + \begin{pmatrix} U_0/c_T & 1 & 0 \\ 1 & U_0/c_T & -U_0/c_T \\ MF \times f_U(U_0)/h_0 & 0 & 0 \end{pmatrix} \frac{\partial}{\partial x_D}\begin{pmatrix} U_D \\ \zeta_D \\ z_{b,D} \end{pmatrix} + \begin{pmatrix} 2gT_T U_0/C^2 h_0 & -c_T T_T U_0^2/C^2 h_0^2 & c_T T_T U_0^2/C^2 h_0^2 \\ 0 & 0 & 0 \\ 0 & 0 & 0 \end{pmatrix} \begin{pmatrix} U_D \\ \zeta_D \\ z_{b,D} \end{pmatrix} = 0 \tag{3.11}$$

where the friction terms can also be written as

$$\frac{2gT_T U_0}{C^2 h_0} = \frac{2g\lambda_T}{C^2 h_0}\frac{U_0}{\sqrt{gh_0}}$$

$$\frac{c_T T_T}{C^2 {h_0}^2} {U_0}^2 = \frac{g\lambda_T}{C^2 h_0}\frac{{U_0}^2}{gh_0}$$

Here the dimensionless parameters are introduced

$$\begin{aligned} Fr &= \frac{U_0}{c_T} && \text{Froude number} \\ \psi &= \frac{f_U(U_0)}{h_0} && \text{dimensionless sediment transport factor} \\ \sigma &= \frac{g\lambda_T}{C^2 h_0} && \text{friction parameter} \end{aligned} \tag{3.12}$$

3.3 Analytical solution

For the equilibrium assumptions, U_0, h_0 are slowly varying which can be assumed to be constant. So F_r, ψ, σ are all locally constant. Then the final dimensionless equations are

$$\begin{aligned} &\frac{\partial}{\partial t_D}\begin{pmatrix} U_D \\ \zeta_D \\ z_{b,D} \end{pmatrix} + \begin{pmatrix} Fr & 1 & 0 \\ 1 & Fr & -Fr \\ MF \times \psi & 0 & 0 \end{pmatrix} \frac{\partial}{\partial x_D}\begin{pmatrix} U_D \\ \zeta_D \\ z_{b,D} \end{pmatrix} \\ &+ \begin{pmatrix} 2\sigma Fr & -\sigma Fr^2 & \sigma Fr^2 \\ 0 & 0 & 0 \\ 0 & 0 & 0 \end{pmatrix} \begin{pmatrix} U_D \\ \zeta_D \\ z_{b,D} \end{pmatrix} = 0 \end{aligned} \tag{3.13}$$

The solution of Equation (3.13) is assumed to have a form like $\phi(x,t) = \hat{\phi(t)} e^{ik_D x_D}$, where k_D is dimensionless wave number for the perturbation and $\phi = \begin{pmatrix} U_D \\ \zeta_D \\ z_{b,D} \end{pmatrix}$. Substitute the solution form into Equation (3.13)

$$\frac{\partial \hat{\phi}(t)}{\partial t} + ik_D A^* \hat{\phi}(t) = 0 \tag{3.14}$$

Where

$$A^* = A + \frac{B}{ik_D}$$

Then

$$A^* = \begin{pmatrix} Fr - i2\sigma Fr/k_D & 1 + i\sigma Fr^2/k_D & -i\sigma Fr^2/k_D \\ 1 & Fr & -Fr \\ MF \times \psi & 0 & 0 \end{pmatrix} \tag{3.15}$$

where σ/k_D represents damping per wave number.

A^* is a 3×3 matrix, so there are three eigenvalues. If the bed is fixed, then there is no sediment transport, i.e. $\psi = 0$. One of the eigenvalues becomes 0, the other two eigenvalues are (without friction)

$$\text{eig}(A^*) = \varphi_{1,2} = Fr \pm 1$$

Where φ is the symbol for eigenvalues Equation (3.3) is the well-known surface wave celerity and they are a function of Froude number only if friction is ignored.

But what still remains unknown is the third eigenvalue which is related to the bed wave, what is the behavior of bed wave to different situation of hydrodynamics and different values of Morfac. Therefore now a mobile bed is considered, $\psi \neq 0$.

Due to the property of eigenvalues and according to Equation (3.14), the following relation holds

$$\frac{d\vec{\phi}}{dt} = -ik_D\varphi\vec{\phi}$$

where $\vec{\phi}$ is an eigenvector of $A*$ and φ is the corresponding eigenvalue. The equation is an ordinary differential equation, which can be easily solved given an initial condition. The solution is

$$\vec{\phi} = C_1 e^{-ik_D\varphi t}$$

where C_1 is a constant determined by the initial conditions. If the eigenvalue φ is a complex number which has the form $\varphi = a + bi$, then

$$\vec{\phi} = C_1 e^{-ik_D(a+bi)t} = C_1 e^{-iak_D t + k_D bt}$$

The real part of the eigenvalue gives the propagation information which is related to the celerity and the imaginary part of the eigenvalue gives the amplification factor.

3.3.1 Stability of Morfac

The imaginary part of the eigenvalues is related to the amplification factor, due to the criteria of stability, the amplitude should be a non-increasing function of time, i.e. $k_D b \leq 0$. Because k_D is taken positive, the imaginary part of the eigenvalues should be negative to fulfill the stability requirements.

$$\text{Stability:} b \leq 0$$

For b should be smaller or equal to zero, the smaller the b, the more damping of amplitude.

3.3.2 Accuracy of Morfac

When Morfac is applied, the sediment transport parameter ψ is directly multiplied by this Morfac hence also the time scale of the bed level change and so should be the eigenvalues for the bed wave. But the surface waves should not be affected by Morfac. If there would be no errors, we would expect the eigenvalue φ_3 to be Morfac times larger than the original eigenvalue, while the surface wave related eigenvalues φ_1 and φ_2 would be unchanged.

$$\varphi_{1,2}(MF) = \varphi_{1,2}(MF = 1) + \text{Errors} \tag{3.16}$$

$$\varphi_3(MF) = MF\varphi_3(MF = 1) + \text{Errors} \tag{3.17}$$

But in a practical view, as long as the errors are small enough, they are acceptable. See Equations (3.16) and (3.17). In order to quantify these

terms the relative amplitude and phase errors can be derived from both surface and bed mode:

For surface waves, (φ_1, φ_2)

- Celerity

$$e_c = 1 - \frac{\Re(\varphi(MF))}{\Re(\varphi(MF = 1))} \tag{3.18}$$

- Amplification

$$e_a = 1 - \frac{\Im(\varphi(MF))}{\Im(\varphi(MF = 1))} \tag{3.19}$$

For bed wave, (φ_3)

- Celerity

$$e_c = 1 - \frac{\Re(\varphi(MF))}{MF \times \Re(\varphi(MF = 1))} \tag{3.20}$$

- Amplification

$$e_a = 1 - \frac{\Im(\varphi(MF))}{MF \times \Im(\varphi(MF = 1))} \tag{3.21}$$

Positive e_c means a lagging phase error and vice versa for a leading phase error. Positive e_a is an overestimation of amplitude and vice versa for an underestimation. These error criteria is only valid when the real part or imaginary part of the eigenvalues are not equal to zero. If the imaginary part of an eigenvalue is zero, then denominators in Equation (3.19) and (3.21) are zero which make the fraction illegal. Better error criteria can be made by combining the imaginary part and real part together, like:

$$\text{Error} = \sqrt{\frac{(a - a_{MF})^2 + (b - b_{MF})^2}{a^2 + b^2}} \tag{3.22}$$

We will use Equation (3.22) for the total error criteria, but for celerity and amplitude error, Equation (3.18) to (3.21) are used. In this thesis, when the real or imaginary part becomes zero, we just defined it as no phase error or no amplitude error.

Phase error indicates how much faster or slower the perturbation propagates, but for the amplitude error, the practical meaning is not that direct, for it is defined on per wavenumber. So it is more convenient to accumulated the amplitude error after one wavelength.

The amplitude has a mode: $e^{bk_D t}$, so the time to propagate one wavelength is :$t = \lambda_T/\Re(\varphi)$, which makes the accumulated amplitude error as:

$$E_a = 1 - \frac{e^{b_{MF} k_D \lambda_T / a_{MF}}}{e^{b k_D \lambda_T / a}} = 1 - \frac{e^{k_T b_{MF}/a_{MF}}}{e^{k_T b/a}} \tag{3.23}$$

Where E_a is the accumulated amplitude error after one wavelength, b_{MF} is the imaginary part of the eigenvalues when applying Morfac, a_{MF} is the real part of the eigenvalues when applying Morfac and k_T is the corresponding typical wavenumber to λ_T. So if $\Re(\varphi)/\Im(\varphi)$ remains the same

$$\varphi(MF = 1) = a + ib$$

$$\varphi(MF) = a_{MF} + ib_{MF}$$

then:

$$\frac{b}{a} = \frac{b_{MF}}{a_{MF}} = \kappa$$

The eigenvector will be:

$$\vec{\phi} = C_1 e^{ik_D(a_{MF} + b_{MF} i)t} = C_1 e^{ik_D(a+bi)\kappa t}$$

Thus the modeling of the physics by Morfac is only accelerated by factor κ slower or faster.

The amplification and celerity are combined together by the ratio: the argument of the complex eigenvalues. In a unidirectional flow situation, the ratio of the celerity and amplitude change for the analytical solution should be constant. As long as the ratio remains the same, only the time scale is adjusted. If the ratio deviates from the analytical solution, then Morfac induce artificial error into the model.

For surface waves, (φ_1, φ_2)

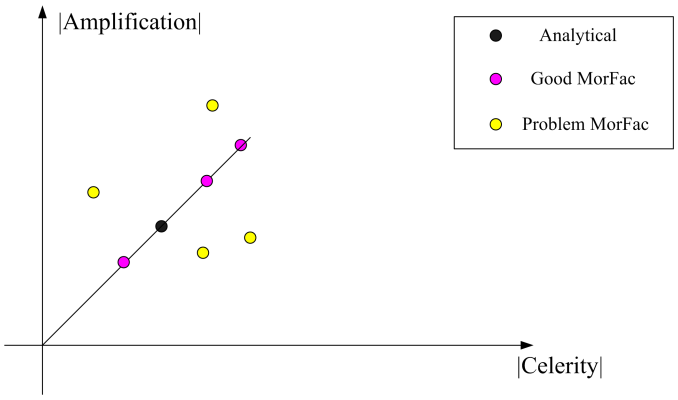

Figure 3.2: *Sketch of ratio of amplitude and celerity*

- Accumulated amplitude error after one wavelength

$$E_a = 1 - \frac{e^{k_T b_{MF}/a_{MF}}}{e^{k_T b/a}} \tag{3.24}$$

For bed wave, (φ_3)

- Accumulated amplitude error after one wavelength

$$E_a = 1 - \frac{e^{k_T b_{MF}/a_{MF}}}{e^{k_T b/a}} \tag{3.25}$$

Moreover, for the accumulated amplitude error, the ration of b/a should be the same for both the surface and bed mode or else the affected timescale for the two modes will be different.

3.3.3 Range of the parameters

The eigenvalues are a function of Froude number, friction parameter, Morfac and ψ. In order to avoid unrealistic hydrodynamic situations, typical engineering scales of the parameters are studied.

1. Froude number: In practical cases, the averaged Froude number is usually smaller than 0.2, but in some shallow areas which is important, it can go up to 0.6.

Table 3.1: *Range of parameters for different situations*

	h(m)	U(m/s)	$\lambda_T(m)$	C	Fr	σ/k_D
Wadden Sea	6.8	1	Large scale:10000 Small scale:50	65	0.12	10(large) 0.003(small)
Western Scheldt	11	1	Large scale:10000 Small scale:50	65	0.1	7(small) 0.002(small)
North Sea	50	0.5	Large scale:10km	65	0.01	0.08

2. ψ: The sediment transport is assumed to be a power function of velocity. Then $S = \alpha U^{\beta}, f_U = \alpha\beta U^{\beta-1}$, ψ is followed by

$$\psi = \frac{\alpha\beta U^{\beta-1}}{h} = \frac{\alpha\beta U^{\beta}}{hU} = \beta\frac{S}{Q}$$

   Where S is the total transport, and Q is the total water discharge, so ψ is proportional to the concentration of the sediment. And in this thesis, according to several test runs, ψ normally lies in the range of 10^{-6} to 10^{-4}.

3. σ: It depends on the λ_T, which is the morphological scale of the model. It could be several meters if a bar movement is considered and several kilometers if an entire tidal basin is modeled.

See Table (3.1), some typical averaged values are chosen for different situations. λ_T is the morphological scale which varies for individual cases. If a small sand wave is modeled, then a typical value for λ_T is around 50 meters. On the other hand, if the entire estuary or tidal basin is modeled, a typical value for λ_T is around 10 kilometers.

3.4 Non-friction case

3.4.1 Solutions

Now, there are four parameters in the system: Froude number, Morfac, ψ, σ. First, the non-friction case, i.e.:$\sigma = 0$ is investigated. The characteristic polynomial of $A*$ is a cubic equation of which the general solution is complex. Maple is used for the analysis. The matrix is:

$$A^* = \begin{pmatrix} Fr & 1 & 0 \\ 1 & Fr & -Fr \\ MF \times \psi & 0 & 0 \end{pmatrix}$$

Several assumptions are made to further simplify the solutions:

1. In the general solution, there is a sign factor, which is $-4 + 8Fr^2 - 4Fr^4 - 36Fr^2MF\psi + 4Fr^4MF\psi + 27MF^2\psi^2Fr^2$, if Froude number, Morfac and ψ is in the range which is discussed before, then the sign factor is negative.

2. The eigenvalues are expanded in a series of Froude number, and higher order of Froude number terms have minor effect if Froude number is smaller than 0.6.

Thus the solutions are :

$$\begin{aligned} \varphi_1 &= 1 + (1 - \frac{1}{2}MF\psi)Fr + (\frac{1}{2}MF\psi - \frac{3}{8}MF^2\psi^2)Fr^2 + \mathrm{O}(Fr^3) \\ \varphi_2 &= -1 + (1 - \frac{1}{2}MF\psi)Fr + (-\frac{1}{2}MF\psi + \frac{3}{8}MF^2\psi^2)Fr^2 + \mathrm{O}(Fr^3) \\ \varphi_3 &= MF\psi Fr + (MF\psi - 2MF^2\psi^2 + MF^3\psi^3)Fr^3 + \mathrm{O}(Fr^5) \end{aligned} \tag{3.26}$$

3.4.2 Stability

From Section 3.3.1, the stability criteria implies that the imaginary part of the eigenvalues should be smaller than one. But in the non-friction case,

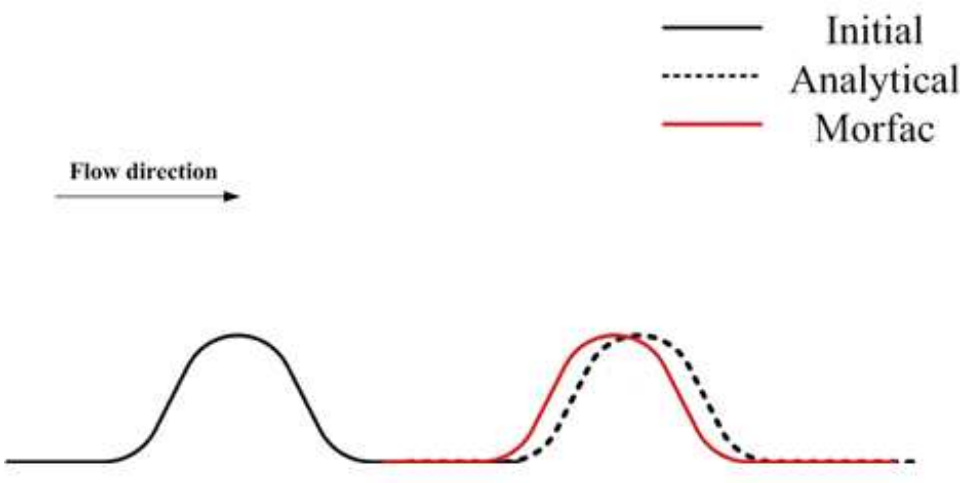

Figure 3.3: *Sketch of lagging phase error without amplitude change*

the eigenvalues approximations are all real numbers, see Equation (3.26). So there is no stability problem in this case.

3.4.3 Accuracy

From Equation (3.26),the real value represents the celerity information. Thus only the celerity error criteria is valid, in this case, there is no amplitude error. In another word, Morfac only accelerates the dynamics, but maybe not at the scale we want. If there is a lagging phase error, the acceleration of Morfac is less than we want. See Figure (3.3).

Phase error on surface

In Equation (3.26), φ_1, φ_2 are surface wave related. If third and higher Froude numbers are neglected, as long as $MF\psi$ is much smaller than 1, then the effect of Morfac on the surface waves is limited. Now Matlab is used to solve the eigenvalues accurately.
In Figure (3.4), the surface waves for $\psi = 10^{-4}$ with different Morfac is plotted. From a broad view, the surface waves after applying Morfac compared to a fixed bed case is almost in a line except when in high

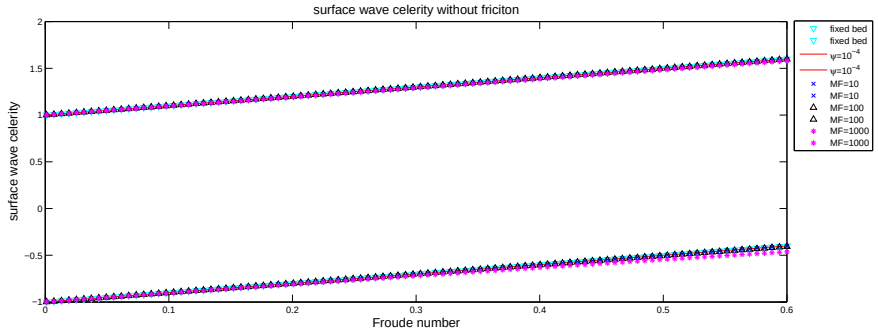

Figure 3.4: *Surface wave celerity without friction*

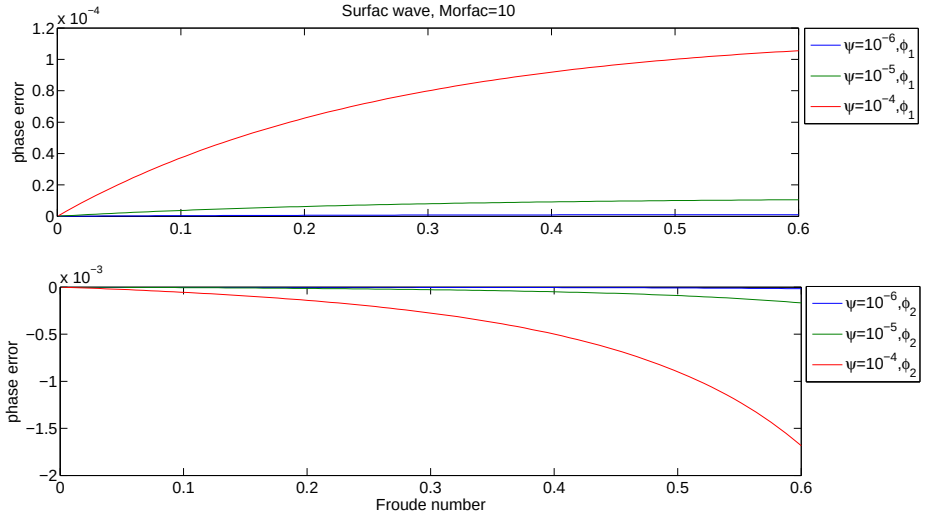

Figure 3.5: *Surface wave phase error without friction*

Froude number region, φ_2 starts to deviate slightly. This is exactly what we see from Equation (3.26). The negative sign in the first order term and the positive in the second order term of Morfac in φ_1 cancels the Morfac effect. However, in φ_2, all the Morfac terms are of negative signs. The magnitude of the surface wave celerity is in the order of 1, the effect of Morfac is also in the order of 1, which is quite large. So a detailed relative phase error is studied based on the error criteria in Section (3.3.2).

From Figure (3.5), with a Morfac of 10, there is a significant phase error combined with large ψ and Froude number. The increase of Froude

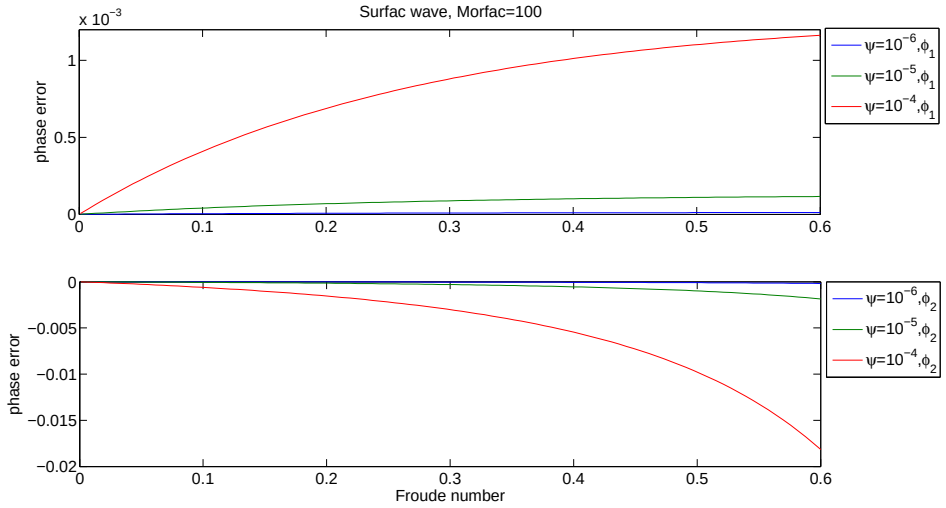

Figure 3.6: *Surface wave phase error without friction*

number and ψ will enlarge the phase error. Normally, φ_2 has a larger error than φ_1. And Morfac induce a lagging phase error on φ_1 and leading on φ_2. See Figure(3.6).

Phase error on bed

From Equation (3.26), if only first order term is considered, Morfac does not induce any error on the bed. An accurate solution is derived.

The same phenomenon is also shown for the phase error on φ_3. Increasing Froude number, ψ and Morfac will increase the bed errors. But the value of the bed phase error is much smaller than that of surface in small Froude number region and around the same order in high Froude number region. So the higher order of Froude number terms in Equation (3.26) is important to the effect of Morfac when the Froude number is large.

Increasing Morfac, ψ, or Froude number can all lead to a larger bed wave phase error. The error on the second surface wave is usually the largest among the three wave modes.

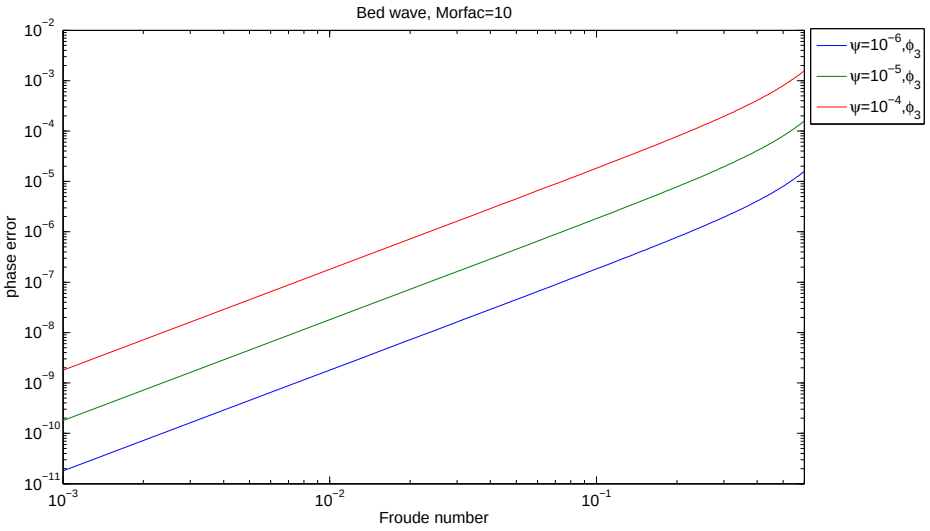

Figure 3.7: *Bed wave phase error without friction*

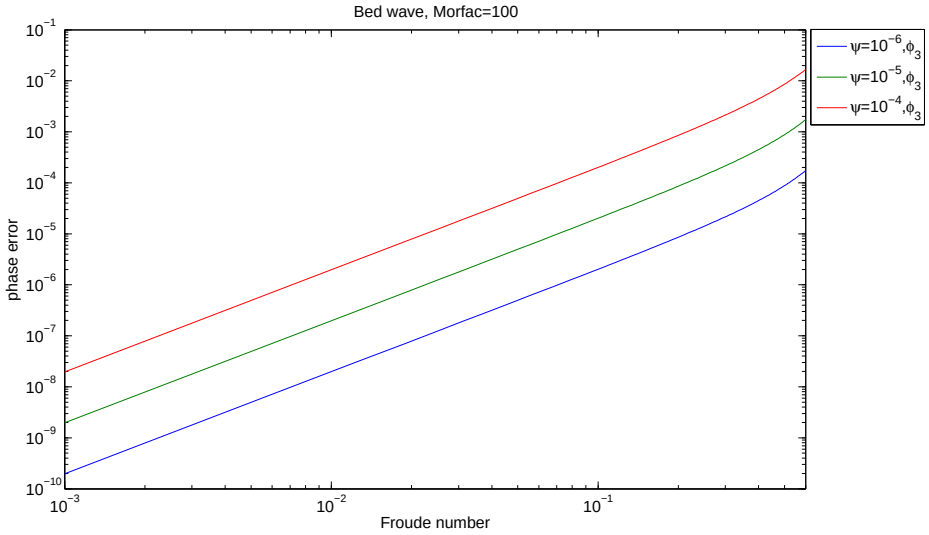

Figure 3.8: *Bed wave phase error without friction*

3.4.4 Critical Morfac

It is hard to define a limit for the error criteria, because in practice, Morfac is not the only contributors to the errors, even the shallow water equation is an approximation to the physical processes. We can't blame an 1% Morfac error with 20% error by the boundary conditions or sediment transport formula. In this thesis, 1% error is chosen as an limit either on surface or bed, and the corresponding Morfac is the critical Morfac to illustrate the relationship between Morfac induced errors with Froude number and ψ.

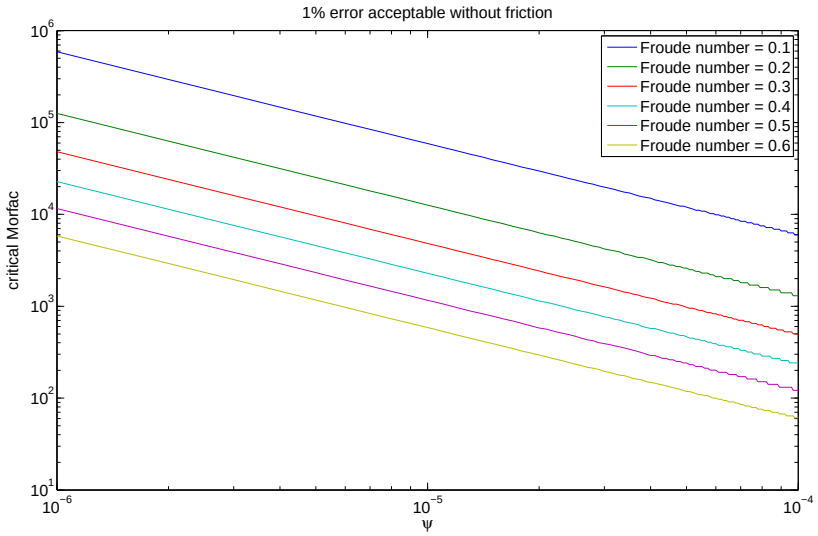

Figure 3.9: *Critical morfac without friction*

Intuitively, from the previously analysis, low ψ or small Froude number can bear larger critical Morfac. The sediment transport factor ψ can be calculated by its physical meaning using flow velocities. If the Englund-Hansen formula is used:

$$S = \alpha U^{\beta}$$

Where S is the sediment transport, U is the flow velocity, β normally equals to 5, and α is a constant of sediment properties.

Froude number	$MF\psi$
0.1	0.589
0.2	0.126
0.3	0.048
0.4	0.023
0.5	0.012
0.6	0.006

Table 3.2: *Upper limit of critical Morfac times ψ to different Froude number*

$$\psi = \frac{\beta S}{Q} \approx 5 \times \frac{2 \times 10^{-5} U^5}{hU} \tag{3.27}$$

Combined the values in Table (3.1), an averaged Froude number of 0.1 can have a critical Morfac of 10^6. But in the shallowest part where the flow velocity is large, Froude number can go to 0.5 or even larger, then the critical Morfac can only be hundred. See Figure (3.9). So Morfac depends hugely on the local environment. If friction is not included, a Morfac of 10^5 in Wadden Sea will only give a 1% lagging bed phase error if the flow velocity is 1m/s and the corresponding $\psi = 2 \times 10^{-6}$. The error induced by Morfac in this case is quite limited.

From Figure (3.9), we can see that the critical Morfac and ψ are highly related. Now we combine them together in order to derive a criteria. A regression analysis in Matlab is done for each Froude number. The expression is assumed to have a form like: $MF \times \psi = \text{Constant}$.

From Table (3.2), the product of Morfac and ψ should be smaller than 0.006 to cover all the range of Froude number. Consequently:

$$MF\psi \leq 0.006, \text{ for } Fr \leq 0.6 \tag{3.28}$$

Equation (3.28) is not always necessary, but always be sufficient in this non-friction case.

3.4.5 Summary

- In the non-friction case, the eigenvalues are all real numbers. The amplitude will not change in this case. There is only a phase error. And it induces a lagging phase error on the bed. For example if a Morfac of 10 in used, the result of the bed evolution would only be an acceleration of the bed wave celerity which is smaller than 10.

- The error induced by Morfac strongly depends on the local environment. Increasing Froude number and ψ will both lead to larger Morfac errors. In small Froude number region, error on the surface wave is much larger than that on the bed wave with the same local environment and Morfac. In higher Froude number region, the error on the bed is nearly in the same order as that on the surface. And φ_2, the surface wave propagates in the opposite direction has the largest error.

- Equation (3.28) enables us to derive a critical Morfac in which only 1% error is induced in the model by Morfac.

3.5 Friction case

From Table (3.1), the friction parameter σ varies with λ_T. In the stability analysis, the system should be stable for all values of σ, but in the accuracy analysis, two cases are studied: large scale case for large friction, and small scale for small friction. Usually, the morphological scale λ_T is coupled with the hydrodynamic wavelength. Long waves are dominant in large scales and short waves in small scales, but the short waves should still be fairly long, otherwise the shallow water equation is not valid.

3.5.1 Solutions

If friction is included, the final Matrix is:

$$A^* = \begin{pmatrix} Fr - iFr2\sigma/k_D & 1 + iFr^2\sigma/k_D & -iFr^2\sigma/k_D \\ 1 & Fr & -Fr \\ MF \times \psi & 0 & 0 \end{pmatrix}$$

Similar assumptions are made as in the non-friction case in order to make Maple analysis:

- The sign factor becomes even more complex in the friction case. But the assumption for a negative value for the sign factor is still valid when the value of Froude number, Morfac and ψ is bounded.
- The eigenvalues are expanded in a series of Froude number.

Then the eigenvalues of the Matrix A^* are:

$$\begin{aligned}
\varphi_1 &= 1 + (1 - \frac{1}{2}MF\psi)Fr - i\frac{\sigma}{k_D}Fr \\
&\quad +(\frac{1}{2}MF\psi - \frac{3}{8}MF^2\psi^2)Fr^2 + (-iMF\psi + \frac{1}{2}i)\frac{\sigma}{k_D}Fr^2 - \frac{1}{2}(\frac{\sigma}{k_D})^2Fr^2 \\
&\quad +O(Fr^3) \\
\varphi_2 &= 1 + (1 - \frac{1}{2}MF\psi)Fr - i\frac{\sigma}{k_D}Fr \\
&\quad +(-\frac{1}{2}MF\psi + \frac{3}{8}MF^2\psi^2)Fr^2 + (iMF\psi - \frac{1}{2}i)\frac{\sigma}{k_D}Fr^2 + \frac{1}{2}(\frac{\sigma}{k_D}^2)Fr^2 \\
&\quad +O(Fr^3) \\
\varphi_3 &= MF\psi Fr \\
&\quad +(MF\psi - 2MF^2\psi^2 + MF^3\psi^3)Fr^3 + (-3iMF\psi + 3iMF^2\psi^2)\frac{\sigma}{k_D}Fr^3 \\
&\quad +O(Fr^5)
\end{aligned} \tag{3.29}$$

Compared with Equation (3.26), in the friction case, not only exists the real part but also the imaginary part in the eigenvalues.

3.5.2 Stability

The stability criteria require the imaginary part of the eigenvalues to be negative for all $\frac{\sigma}{k_D}$. If only first and second order Froude number terms are taken into account.

$$\Im(\varphi_1) \approx -\frac{\sigma}{k_D}Fr + (-MF\psi\frac{\sigma}{k_D} + \frac{1}{2}\frac{\sigma}{k_D})Fr^2 < 0 \Rightarrow (\frac{1}{2} - MF\psi)Fr < 1$$
$$\Im(\varphi_2) \approx -\frac{\sigma}{k_D}Fr + (MF\psi\frac{\sigma}{k_D} - \frac{1}{2}\frac{\sigma}{k_D})Fr^2 < 0 \Rightarrow (MF\psi - \frac{1}{2})Fr < 1$$
$$\Im(\varphi_3) \approx (-3MF\psi\frac{\sigma}{k_D} + 3MF^2\psi^2\frac{\sigma}{k_D})Fr^3 < 0 \Rightarrow MF\psi < 1$$

φ_1 is stable for all cases, but φ_2 and φ_3 become unstable, when $\psi \times MF$ is large. Because in practice, sediment transport factor normally cannot go up to 10^{-3}, without applying Morfac, the analytical model is always stable. But with a Morfac of 10^4 and a ψ of 10^{-4}, φ_3 will become unstable. Morfac does induce instability even in the analytical model.

3.5.3 Accuracy: Moderate friction case

When friction is included, there is not only a phase error, but also an amplitude error. The detailed criteria is based on Section (3.3.1). As long as Froude number or σ/k_D becomes large, friction will be important. So to the small friction case, it is more or less similar to the non-friction case. In order to see the effect of friction, first moderate friction is analyzed, it is combined with moderate morphological scale and relatively short waves. For simplicity, σ/k_D is chosen as 1.

Phase error on surface waves

From Equation (3.29), we can see that the friction term not only influences imaginary part but also the real part. So it affects the surface wave celerity. Accurate solutions are derived by Matlab.

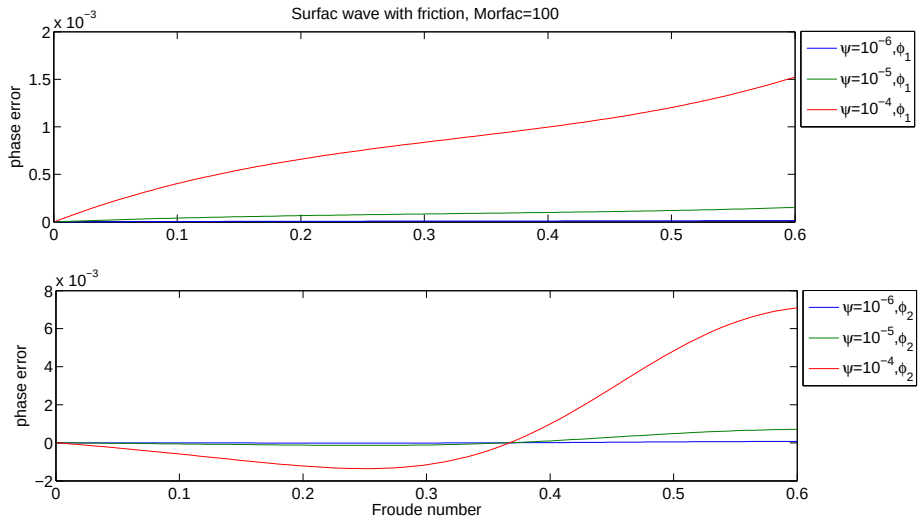

Figure 3.10: *Phase error on surface waves with moderate friction (σ/k_D=1)*

Figure (3.10) shows the phase error on surface waves when moderate friction is considered. Compared to the non-friction case, the trend of φ_1 has rarely any differences, but the value of error increases. It also has a lagging phase error. To φ_2, friction comes into effect when Froude number is larger than 0.3. In low Froude number region, φ_2 has a leading phase error, when friction becomes important, it shows a lagging phase error, which means the effect of friction on the surface wave propagation is overestimated. Meanwhile, the value of error for φ_2 decreases. So friction tends to make a lagging phase on the surface, which increases the original lagging phase error but decreases the leading phase error.

Phase error on bed wave

From Equation (3.29), we can see the expression for φ_3 the real part is nearly the same as in the non-friction case if higher order terms are neglected.

But the accurate solutions solved by Matlab (see Figure (3.11)) shows a different phenomenon. Friction also becomes important when Froude

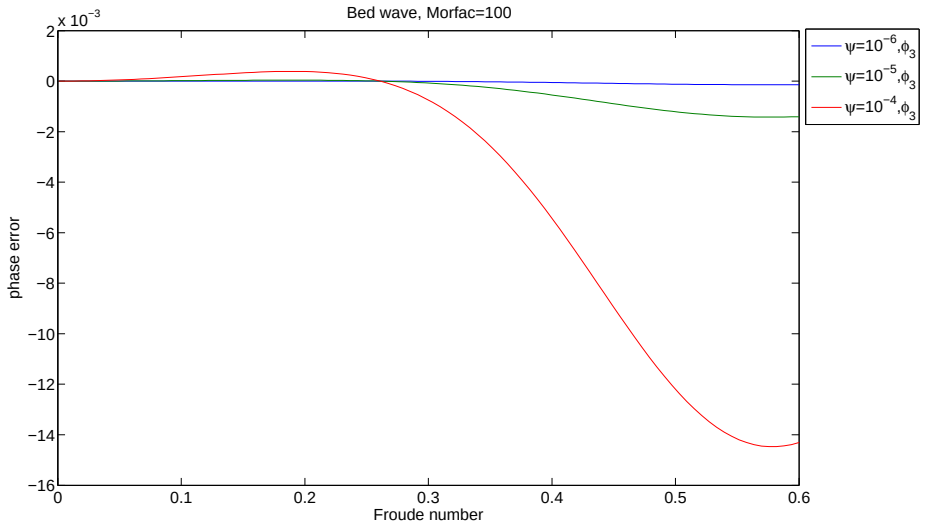

Figure 3.11: *Phase error on bed waves with moderate friction,(σ/k_D=1)*

number is larger than 0.3. Different from the surface waves, the phase error becomes a leading phase error from original lagging phase. The absolute value of the phase error on bed is also decreased. So the effect of friction to the celerity also becomes important in higher Froude number range.

Amplitude error on surface waves

The imaginary part of the eigenvalues are investigated. The criteria is based on Equation (3.19) and (3.21). The effect of friction term to φ_1 and φ_2 are different while φ_1 shows an overestimate of amplitude and φ_2 for an underestimate. This can be seen from Equation (3.29). The sign of the imaginary part for φ_1 and φ_2 are different. See Figure (3.12)

Amplitude error on bed wave

In Figure (3.13), friction also interfere the amplitude of the bed waves. And the error is large compared to others, almost 1 percent per wave number. In higher Froude number region, the error becomes negative, and shows an underestimate of the amplitude.

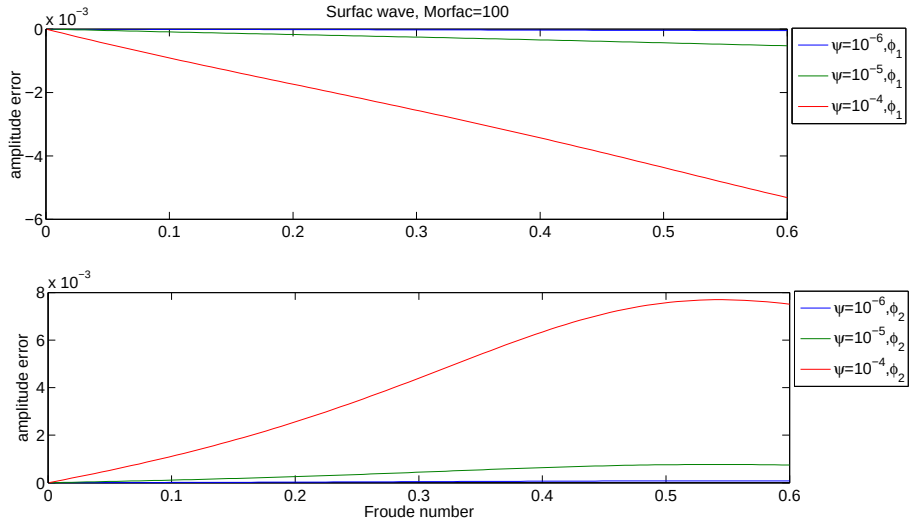

Figure 3.12: *Amplitude error on surface waves with moderate friction,(σ/k_D=1)*

Total error

If the amplitude error and the phase error is simply combined by Equation (3.23), we will see that value of the total error is larger than the phase error alone in the non-friction case when Froude number is small.
In Figure (3.14) and (3.15), the accumulated amplitude error for surface and bed wave are shown. The main effect of friction is it damps out the error in high Froude number region.

3.5.4 Accuracy:Large friction case

The same analysis is done for the large friction case, combined with long waves and large morphological scale. Here the damping per wavenumber is $\sigma/k_D = 10$.
Not all the error is going to studied, only the total error is investigated, for it is a combination of the amplitude and celerity.
From Figure (3.16), compared to the moderate friction case, friction comes into effect even in small Froude number region, and the magnitude of the

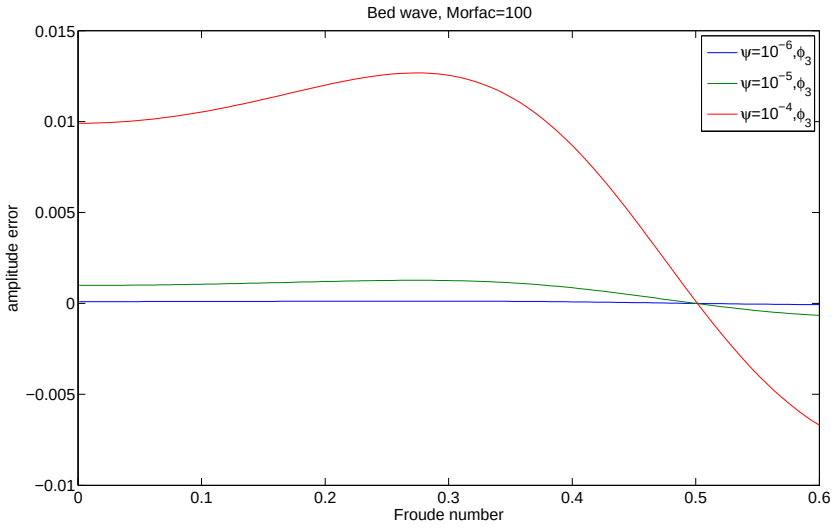

Figure 3.13: *Amplitude error on bed waves with moderate friction,(σ/k_D=1)*

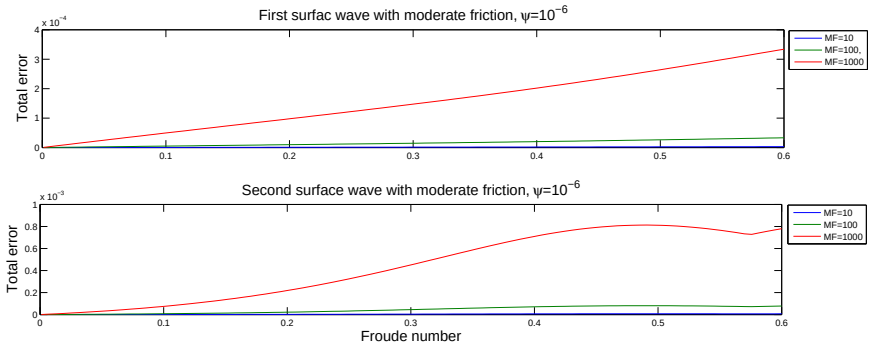

Figure 3.14: *Total surface error for moderate friction case, (σ/k_D=1,$\psi = 10^{-6}$)*

errors are much smaller in high Froude number region.

A different effect is shown for the bed waves, see Figure (3.17). There are two peaks in the figure. One is caused by the largest celerity error, the other is caused by the largest amplitude error.

When Froude number becomes large, the effect of friction is important.

3.5.5 Critical Morfac

The same criteria is used as for the non-friction case: 1% error is acceptable either on surface wave or bed wave. But now the error is

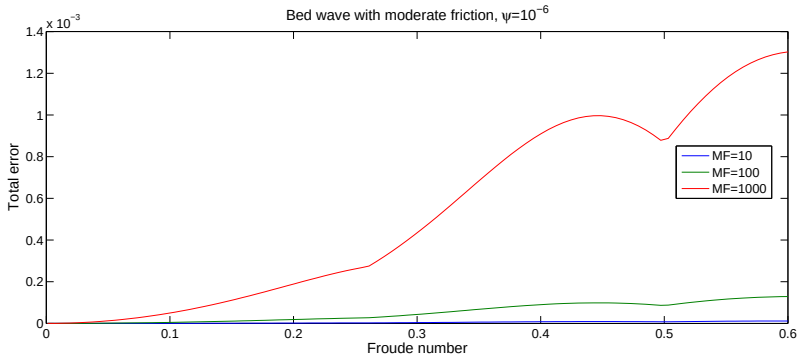

Figure 3.15: *Total bed error for moderate friction case,(σ/k_D=1,$\psi = 10^{-6}$)*

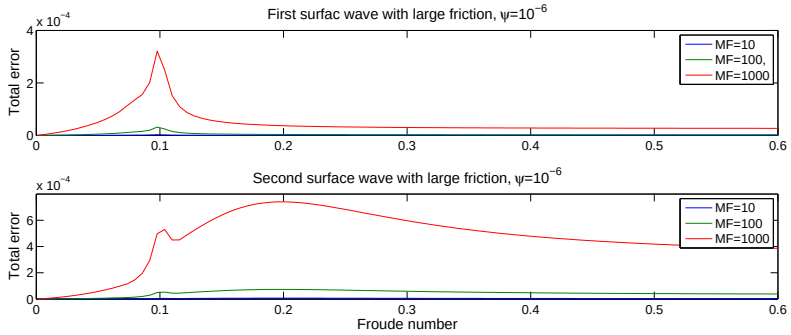

Figure 3.16: *Total surface error for large friction case, (σ/k_D=10,$\psi = 10^{-6}$)*

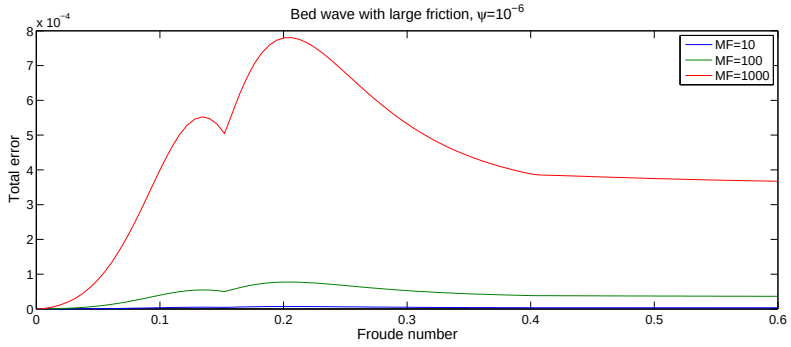

Figure 3.17: *Total bed error for large friction case,(σ/k_D=10,$\psi = 10^{-6}$)*

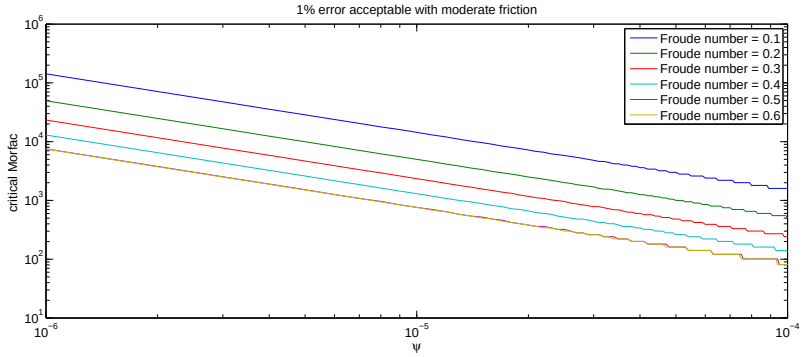

Figure 3.18: *Critical Morfac for moderate friction,(σ/k_D=1)*

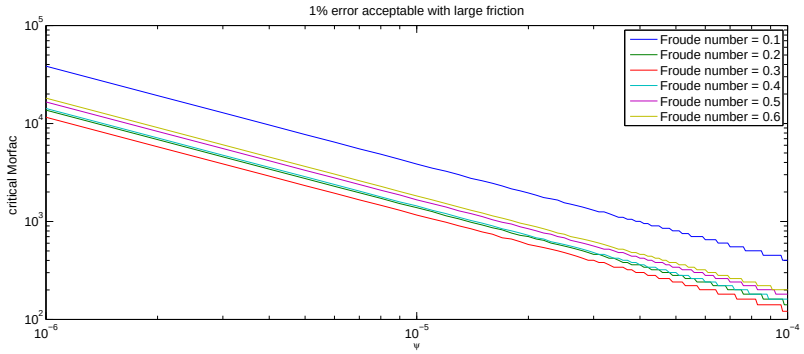

Figure 3.19: *Critical Morfac for large friction,(σ/k_D=10)*

calculated by the total error because it combines both the celerity and the amplitude. In low Froude number region, φ_2 gives larger error. But in the high Froude number region, φ_3 usually gives the largest error among the three.

Figure (3.18) gives a similar graph like the non-friction case. But the value of critical Morfac is smaller than non-friction case in small Froude number but larger in large Froude number. The reason is that friction will become important in high Froude number region, and the errors are damped out by friction.

In the large friction case, the phenomenon is similar to the moderate friction case, but it seems that the Froude number is not important anymore. The lines for different Froude numbers overlapped each other. A

Froude number	$MF\psi$ (small scale)	$MF\psi$ (large scale)
0.1	0.1427	0.04
0.2	0.049	0.014
0.3	0.023	0.012
0.4	0.013	0.014
0.5	0.008	0.016
0.6	0.007	0.018

Table 3.3: *Upper limit of critical Morfac times ψ to different Froude number with friction*

Table 3.4: *Critical Morfac in the most severe situations for three locations based on total errors*

	Froude number	ψ	Morfac
Wadden Sea	0.3	1×10^{-5}	Large: 1100 Small:3000
Western Scheldt	0.4	3×10^{-5}	Large:480 Small:580
North Sea	0.1	10^{-6}	16000

table of the upper limit for the product of Morfac and ψ with different Froude number and friction is shown below by doing the same regression analysis in the non-friction case. See Table (3.3). Smaller critical Morfac can be derived in large friction case when Froude number is smaller. But in high Froude number region, it is larger than the moderate friction and non-friction case.

$$\begin{aligned} MF \times \psi &\leq 0.007(\text{Small scale}) \\ MF \times \psi &\leq 0.018(\text{Large scale}) \end{aligned} \tag{3.30}$$

Based on these two graphs, a critical Morfac is derived in Table (3.4) for three different situations from Table (3.1).

If only the amplitude errors are focused instead of total errors:

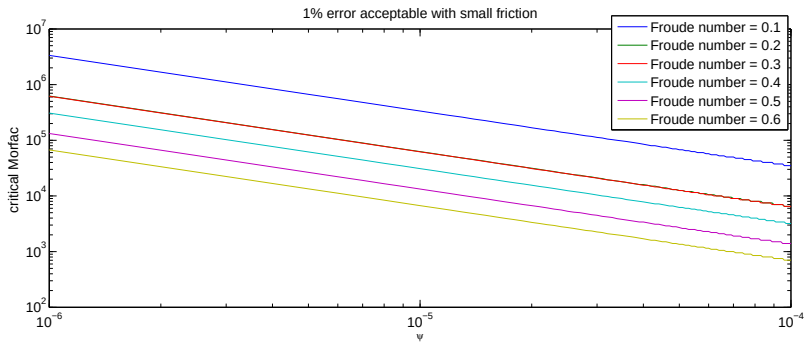

Figure 3.20: *Critical Morfac for moderate friction using accumulated amplitude error,(σ/k_D=1)*

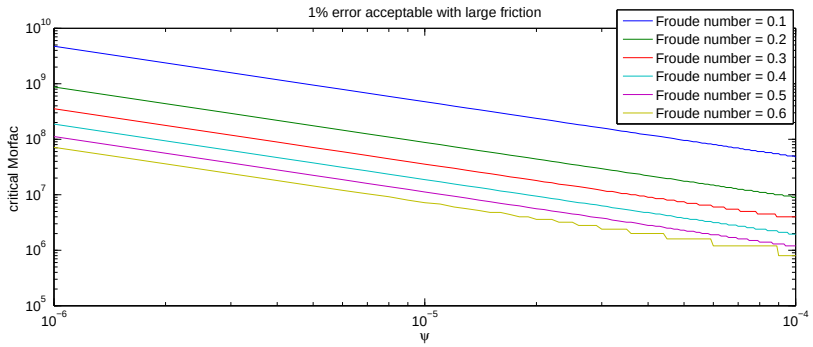

Figure 3.21: *Critical Morfac for large friction using accumulated amplitude error,(σ/k_D=1)*

As we can see from Figure (3.20) and (3.21), all the critical Morfac is larger than that based on the total errors. Large friction can have larger critical Morfac than small friction, when Froude number and ψ are the same. And amplitude errors are related to stability, in other words, large friction cases are more stable than small friction cases.

The effect of friction is different for stability and accuracy. Larger friction case will give larger total errors but more stable model than smaller friction cases.

3.5.6 Limitation of the analysis

From Table (3.4), the critical Morfac is larger than we used in practice. Some difference between the analysis and practice may overestimate the critical Morfac values here.

- Only a single event is considered here. But in practice, the combination of different events may lower the critical Morfac.

- The assumption of unidirectional flow in analysis instead of time dependent flow may also increase the critical Morfac value.

- Bed-load sediment transport formula is used here. In practice, suspended load may decrease the critical Morfac.

- Uniform variables are used in the analysis. Non-uniformity may also decrease the critical Morfac.

3.5.7 Summary

- The eigenvalues become complex when friction is included. In low Froude number region, when σ/k_D is small, the error phenomenon is similar to the non-friction case. In high Froude number region, the phenomenon will be changed by friction. The effect of friction is not the same to the three eigenvalues.

- Similar error relationship is shown as the non-friction case. Larger ψ and Morfac will all indicate large errors. Large friction cases will give more stable model, but less accuracy than small friction. Overall, See Table (3.5):

Table 3.5: *Summary of the error*

	Amplitude	Phase
φ_1	Underestimate	Lagging
φ_2	Overestimate	Leading (Low Froude), Lagging (High Froude)
φ_3	Overestimate(Low Froude), Underestimate(High Froude)	Lagging (Low Froude), Leading (High Froude)

3.6 Conclusions

The eigenvalue analysis is applied to analyze the propagation of the perturbation for the analytical model. Both the celerity and the amplitude error on the surface and bed are studied.

1. Morfac will not induce stability problem in the analytical model unless unreasonable large Morfac is chosen which leads to $MF \times \psi \geq 1$.

2. Morfac does not only affect the accuracy of bed wave but also of the surface waves. When friction is not considered, Morfac induces phase errors while the amplitude is also affected when friction is included.

3. Froude number and ψ are dominant factors for Morfac induced errors. Larger Froude number and ψ will usually lead to large Morfac errors.

4. Friction is good for stability but not for accuracy.

Chapter 4

Analysis of numerical implementation of Morfac

The shallow water equations well describe the physical processes in coastal or nearshore areas, however, they are so difficult to be solved analytically, therefore numerical approximations are necessary. As long as the numerical errors are smaller or the same order as the errors in the analytical model, the numerical approximations are considered good enough.
The following discretisation is similar to the current Delft3D-FLOW but friction term will not included for simplicity. After studying the numerical model, we are able to understand the effect of model properties, such as Courant number and points per wave length .

4.1 Background

4.1.1 Staggered grid

The numerical method of Delft-FLOW is based on finite differences. The primitive variables water level ζ and velocity U describe the flow, and the bed level z_b describes the morphology. To discretize the shallow water

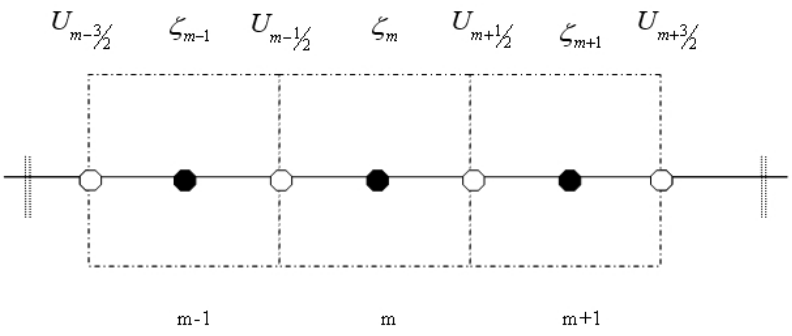

Figure 4.1: *Staggered grid*

equations, the variables are arranged in a specific way on the grid, see Figure 4.1. The water depth and bed level points are defined in the center of a cell, meanwhile the velocity components are located at the grid cell faces. This pattern is called a staggered grid. Uniform grid size is assumed here.

Staggered grids have been extensively used thanks for the advantages like: simple implementation on boundaries, less variables than non-staggered grids to achieve the same accuracy and exclusion of spurious oscillations.

4.1.2 ADI time integration method

Leedertse (1967) introduced an Alternating Direction Implicit (ADI) method for shallow water equation. It is a computationally efficient time intergration method applied in Delft3D-FLOW. The ADI method splits one time step into two stages where each stage consists of half a time step. In both stages, all the terms of the model equations are solved in a consistent way with second-order accuracy in space. Both for the water level gradient and the advection terms, the time levels are alternating. If in one stage the term is taken implicitly in time, in the other stage it will

be explicit. Except the bed level friction and viscosity term, they are always implicit for stability reasons.

4.2 Discretization the equations

The equations for the point m and time level p read (if friction is neglected):

Stage 1:

$$\begin{aligned} &S_t(U^{p+\frac{1}{2}}_{m+\frac{1}{2}}) + U^p_{m+\frac{1}{2}} S_{1x}(U^p_{m+\frac{1}{2}}) + gS_{0x}(\zeta^{p+\frac{1}{2}}_{m+\frac{1}{2}}) = 0 \\ &S_t(\zeta^{p+\frac{1}{2}}_m) + S_{0x}(h^{p+\frac{1}{2}}_m U^{p+\frac{1}{2}}_m) = 0 \\ &S_t(z^{p+\frac{1}{2}}_{b,m}) + MF \times S_{0x}(S^p_m) = 0 \end{aligned} \tag{4.1}$$

Stage 2:

$$\begin{aligned} &S_t(U^{p+1}_{m+\frac{1}{2}}) + U^{p+\frac{1}{2}}_{m+\frac{1}{2}} S_{+x}(U^{p+1}_{m+\frac{1}{2}}) + gS_{0x}(\zeta^{p+\frac{1}{2}}_{m+\frac{1}{2}}) = 0 \\ &S_t(\zeta^{p+1}_m) + S_{0x}(h^{p+\frac{1}{2}}_m U^{p+\frac{1}{2}}_m) = 0 \\ &S_t(z^{p+1}_{b,m}) + MF \times S_{0x}(S^{p+\frac{1}{2}}_m) = 0 \end{aligned} \tag{4.2}$$

Where the derivatives are represented by:

$$\begin{aligned} &S_t(U^{p+\frac{1}{2}}_{m+\frac{1}{2}}) = (U^{p+\frac{1}{2}}_{m+\frac{1}{2}} - U^p_{m+\frac{1}{2}})/\frac{1}{2}\Delta t \\ &S_t(\zeta^{p+\frac{1}{2}}_m) = (\zeta^{p+\frac{1}{2}}_m - \zeta^p_m)/\frac{1}{2}\Delta t \\ &S_t(z^{p+\frac{1}{2}}_{b,m}) = (z^{p+\frac{1}{2}}_{b,m} - z^p_{b,m})/\frac{1}{2}\Delta t \\ &S_{1x}(U^p_{m+\frac{1}{2}}) = (U^p_{m+\frac{3}{2}} - U^p_{m-\frac{1}{2}})/2\Delta x \\ &S_{0x}(\zeta^{p+\frac{1}{2}}_{m+\frac{1}{2}}) = (\zeta^{p+\frac{1}{2}}_{m+1} - \zeta^{p+\frac{1}{2}}_m)/\Delta x \\ &S_{0x}(h^{p+\frac{1}{2}}_m U^{p+\frac{1}{2}}_m) = (h^{p+\frac{1}{2}}_{m+\frac{1}{2}} U^{p+\frac{1}{2}}_{m+\frac{1}{2}} - h^{p+\frac{1}{2}}_{m-\frac{1}{2}} U^{p+\frac{1}{2}}_{m-\frac{1}{2}})/\Delta x \\ &S_{0x}(S^{p+\frac{1}{2}}_m) = (S^p_{m+\frac{1}{2}} - S^p_{m-\frac{1}{2}})/\Delta x = S^p_{m+1} - S^p_{m-1}/2\Delta x \\ &S_{+x}(U^{p+1}_m) = \begin{cases} 3U^{p+1}_{m+\frac{1}{2}} - 4U^{p+1}_{m-\frac{1}{2}} + U^{p+1}_{m-\frac{3}{2}}/2\Delta x & U^p_{m+\frac{1}{2}} > 0 \\ -3U^{p+1}_{m+\frac{2}{5}} + 4U^{p+1}_{m+\frac{2}{3}} - U^{p+1}_{m+\frac{1}{2}}/2\Delta x & U^p_{m+\frac{1}{2}} < 0 \end{cases} \end{aligned}$$

Δx is the grid size and Δt is the time step.

4.3 von-Neuman stability analysis

Von-Neuman stability analysis (also called Fourier stability analysis) is a procedure used to check the stability of finite difference schemes as applied to a system of linearized partial differential equations. Both the internal scheme and the boundary scheme will influence the stability of the Delft3D model. But now only internal scheme is focused because boundaries are not involved in the von-Neuman analysis. In this way the necessary conditions for stability are obtained. But in practice, still some stability problems will show up due to the boundary problems, non-linear effects or non-uniform grid effects which are not included in this analysis. It utilizes the assumption that separation of variables can be used to express the solution in time and space, and thus can be represented by a Fourier series expansion. The key to the analysis is that the linearity of the differential equation allows one to examine a single Fourier component of the solution at a time. For the discretized shallow water equation have non-linear terms. The first step is to do a perturbation analysis to linearize the equations.

4.3.1 Small perturbation analysis

The shallow water equations are a set of non-linear partial differential equations. In order to study the stability, linearization by small perturbation analysis is similar to procedure in Section (3.2). A small

perturbation from initially equilibrium situation is assumed:

$$U^p = U_0^p + U'^p$$
$$\zeta^p = \zeta_0^p + \zeta'^p$$
$$z_b^p = z_{b,0}{}^p + z_b'^p$$
$$S^p = S_0^p + S'^p$$

This yields:

Stage 1:

$$S_t((U_0+U')^{p+\frac{1}{2}}_{m+\frac{1}{2}}) + ((U_0+U')^p_{m+\frac{1}{2}})S_{1x}((U_0+U')^p_{m+\frac{1}{2}}) + gS_{0x}((\zeta_0+\zeta')^{p+\frac{1}{2}}_{m+\frac{1}{2}}) = 0$$
$$S_t((\zeta_0+\zeta')^{p+\frac{1}{2}}_m) + S_{0x}((h_0+h')^{p+\frac{1}{2}}_m(U_0+U')^{p+\frac{1}{2}} + m) = 0$$
$$S_t((z_{b,0}+z_b')^{p+\frac{1}{2}}_m) + MF \times S_{0x}((S_0+S')^p_m) = 0$$

Stage 2:

$$S_t((U_0+U')^{p+1}_{m+\frac{1}{2}}) + ((U_0+U')^{p+\frac{1}{2}}_{m+\frac{1}{2}})S_{+x}((U_0+U')^{p+1}_{m+\frac{1}{2}}) + gS_{0x}((\zeta_0+\zeta')^{p+\frac{1}{2}}_{m+\frac{1}{2}}) = 0$$
$$S_t((\zeta_0+\zeta')^{p+1}_m) + S_{0x}((h_0+h')^{p+\frac{1}{2}}_m(U_0+U')^{p+\frac{1}{2}}_m) = 0$$
$$S_t((z_b,0+z')^{p+1}_m) + MF \times S_{0x}((S_0+S')^{p+\frac{1}{2}}_m) = 0$$

For the equations in Stage 1, the background solutions are (assuming $U^p_{m+\frac{1}{2}} > 0$):

$$\text{Momentum equation, point}(m+\tfrac{1}{2}): \quad S_t(U_0^{p+\frac{1}{2}}) + (U_0^{p+\frac{1}{2}})S_{1x}(U_0^p) + gS_{0x}(\zeta_0^{p+\frac{1}{2}}) = 0$$
$$\text{Continuity equation, point}(m): \quad S_t(\zeta_0^{p+\frac{1}{2}}) + S_{0x}(h^{p+\frac{1}{2}}U_0^{p+\frac{1}{2}}) = 0$$
$$\text{Morphology change, point}(m): \quad S_t(z_{b,0}^{p+\frac{1}{2}}) + MF \times S_{0x}(S_0^{p+\frac{1}{2}}) = 0$$

The linearization of the momentum equation is investigated in detail. $U'^pS_{1x}(U_0^p)$ and $U'^pS_{1x}(U'^p)$ are all small perturbations compared to $U_0^pS_{1x}(U'^p)$ which are neglected. So the linearized equation is:

$$S_t(U'^{p+\frac{1}{2}}_{m+\frac{1}{2}}) + (U^p_{0,m+\frac{1}{2}})S_{1x}(U'^p_{m+\frac{1}{2}}) + gS_{0x}(\zeta'^{p+\frac{1}{2}}_{m+\frac{1}{2}}) = 0$$

The same for reasoning for the continuity equation and the bed level change equations applies. (See Appendix A) U_0 is slow varying for the

equilibrium situation, so U_0^p assumed constant. To linearize the sediment transport term: S is assumed to be a function of velocity only.

$$S_{m+1}^p - S_{m-1}^p = f_U \times (U_{m+\frac{3}{2}}^p + U_{m+\frac{1}{2}}^p - U_{m-\frac{1}{2}}^p - U_{m+\frac{3}{2}}^p)/2$$

This yields the following reduced scheme: Stage 1:

$$\begin{aligned}
&S_t(U_{m+\frac{1}{2}}^{\prime p+\frac{1}{2}}) + U_0 S_{1x}(U_{m+\frac{1}{2}}^{\prime p}) + g S_{0x}(\zeta_{m+\frac{1}{2}}^{\prime p+\frac{1}{2}}) = 0\\
&S_t((\zeta_m^{\prime p+\frac{1}{2}}) + h_0 S_{0x}(U_m^{\prime p+\frac{1}{2}}) + U_0 S_{0x}(h_m^{\prime p+\frac{1}{2}}) = 0\\
&S_t(z_{bm}^{\prime\, p+\frac{1}{2}}) + MF \times f_{U0} \times S_x(U_m^{\prime p}) = 0
\end{aligned}$$

Stage 2:

$$\begin{aligned}
&S_t(U_{m+\frac{1}{2}}^{\prime p+1}) + U_0 S_{+x}(U_{m+\frac{1}{2}}^{\prime p+1}) + g S_{0x}(\zeta_{m+\frac{1}{2}}^{\prime p+\frac{1}{2}}) = 0\\
&S_t(\zeta_m^{\prime p+1}) + U_0 S_{0x}(h^{\prime})_m^{p+\frac{1}{2}} + h_0 S_{0x}(U_m^{\prime p+\frac{1}{2}}) = 0\\
&S_t(z_{b,m}^{\prime\ p+1}) + MF \times f_{U0} \times S_x(U_m^{\prime p+\frac{1}{2}}) = 0
\end{aligned}$$

where $S_x(U_m^{\prime p}) = f_U \times (U_{m+\frac{3}{2}}^{\prime p} + U_{m+\frac{1}{2}}^{\prime p} - U_{m-\frac{1}{2}}^{\prime p} - U_{m+\frac{3}{2}}^{\prime p})/(2\Delta x)$
The solutions of the system in time level p and point m are assumed in the form of:

$$\varepsilon_m^p = \hat{\varepsilon}^p e^{imk\Delta x}$$

where

$$\varepsilon = \begin{pmatrix} U^{\prime} \\ \zeta^{\prime} \\ z_b^{\prime} \end{pmatrix}$$

The water depth at point m+1/2 in Delft3D is defined as the minimum of the adjacent depth at water level points. :

$$h_{m+\frac{1}{2}}^p = \zeta_m - \min(z_{b,m+1}, z_{b,m})$$

So if the water depth is decreasing in the flow direction, the bed level is taken as downwind instead of upwind. As we know, a downwind scheme is unconditionally unstable which will show later. But now we only stick to the upwind scheme. Further substitution leads to:

Stage 1:

$$\hat{U}'^{p+\frac{1}{2}} + \frac{g\Delta t i \sin\frac{1}{2}k\Delta x}{\Delta x}\hat{\zeta}'^{p+\frac{1}{2}} = (1 - \frac{U_0\Delta t i \sin k\Delta x}{2\Delta x})\hat{U}'^{p}$$
$$\frac{(\zeta_0 - z_{b,0})\Delta t i \sin\frac{1}{2}k\Delta x}{\Delta x}\hat{U}'^{p+\frac{1}{2}} + (1 + \frac{U_0\Delta t(1 - e^{ik\Delta x})}{2\Delta x})\hat{\zeta}'^{p+\frac{1}{2}}$$
$$-\frac{U_0\Delta t(1 - e^{ik\Delta x})}{2\Delta x}\hat{z_b'}^{p+\frac{1}{2}} = \hat{\zeta}'^{p}$$
$$\hat{z_b'}^{p+\frac{1}{2}} = \hat{z_b'}^{p} - MF \times \frac{f_{U0}\Delta t i(\sin\frac{1}{2}k\Delta x + \sin\frac{3}{2}k\Delta x)}{4\Delta x}\hat{U}'^{p}$$

Stage 2:

$$\hat{U}'^{p+1}(1 + \frac{U_0\Delta t(3 - 4e^{-ik\Delta x} + e^{-2ik\Delta x})}{4\Delta x}) = \hat{U}'^{p+\frac{1}{2}} - \frac{g\Delta t i \sin\frac{1}{2}k\Delta x}{\Delta x}\hat{\zeta}'^{p+\frac{1}{2}}$$
$$\hat{\zeta}'^{p+1} = -\frac{(\zeta_0 - z_{b,0})\Delta t i \sin\frac{1}{2}k\Delta x}{\Delta x}\hat{U}'^{p+\frac{1}{2}} - (1 + \frac{U_0\Delta t(1 - e^{ik\Delta x})}{2\Delta x})\hat{\zeta}'^{p+\frac{1}{2}}$$
$$+\frac{U_0\Delta t(1 - e^{ik\Delta x})}{2\Delta x}\hat{z_b'}^{p+\frac{1}{2}}$$
$$\hat{z_b'}^{p+1} = \hat{z_b'}^{p+\frac{1}{2}} - MF \times \frac{f_{U0}\Delta t i(\sin\frac{1}{2}k\Delta x + \sin\frac{3}{2}k\Delta x)}{4\Delta x}\hat{U}'^{p+\frac{1}{2}}$$

4.3.2 Non-dimensionlized equations

As discussed in Chapter 3, dimensionless systems give better insight in the relative importance of different factors. So typical length scale and velocity scale are introduced to non-dimensionlized the equations:

$$U' = \sqrt{gh_0}U_D,$$
$$\zeta' = h_0\zeta_D,$$
$$z_b' = h_0 z_{b,D}$$

The dimensionless parameters are defined as follow:

Froude number:	$Fr = U_0/\sqrt{gh_0}$
Dimensionless sediment transport:	$\psi = f_{U0}/h_0$
Points per wavelength:	$N = L/\Delta x \quad n = 2\pi/N$
Courant number:	$Cr = \sqrt{gh_0}\Delta t/\Delta x$

Stage 1:

$$\hat{U_D}^{p+\frac{1}{2}} + Cr \times i \sin\frac{1}{2} n \hat{\zeta_D}^{p+\frac{1}{2}} = (1 - Cr \times Fr \times \frac{i \sin n}{2}) \hat{U_D}^{p}$$

$$Cri \sin\frac{1}{2} n \hat{U_D}^{p+\frac{1}{2}} + (1 + Cr \times Fr \times \frac{1 - e^{-in}}{2}) \hat{\zeta_D}^{p+\frac{1}{2}} - Cr \times Fr \times \frac{1 - e^{-in}}{2} \hat{z_D}^{p+\frac{1}{2}} = \hat{\zeta_D}^{p}$$

$$\hat{z_D}^{p+\frac{1}{2}} = \hat{z_D}^{p} - \frac{1}{4} MF \times Cr \times \psi \times i(\sin\frac{1}{2} n + \sin\frac{3}{2} n) \hat{U_D}^{p+\frac{1}{2}}$$

Stage 2:

$$(1 + \frac{Fr \times Cr \times (3 - 4e^{-in} + e^{-2in})}{4}) \hat{U_D}^{p+1} = \hat{U_D}^{p+\frac{1}{2}} - Cri \sin\frac{1}{2} n \hat{\zeta_D}^{p+\frac{1}{2}}$$

$$\hat{\zeta_D}^{p+1} = -Cr \times i \sin\frac{1}{2} n \hat{U_D}^{p+\frac{1}{2}} + (1 - Fr \times Cr \times \frac{1 - e^{-in}}{2}) \hat{\zeta_D}^{p+\frac{1}{2}} + Fr \times Cr \times \frac{1 - e^{-in}}{2} \hat{z_{b,D}}^{p+\frac{1}{2}}$$

$$\hat{z_{b,D}}^{p+1} = \hat{z_{b,D}}^{p+\frac{1}{2}} - \frac{1}{4} MF \times Cr \times \psi \times i(\sin\frac{1}{2} n + \sin\frac{3}{2} n) \hat{U_D}^{p+1}$$

In the matrix form:

$$A \begin{pmatrix} \hat{U_D}^{p+\frac{1}{2}} \\ \hat{\zeta_D}^{p+\frac{1}{2}} \\ \hat{z_D}^{p+\frac{1}{2}} \end{pmatrix} = B \begin{pmatrix} \hat{U_D}^{p} \\ \hat{\zeta_D}^{p} \\ \hat{z_D}^{p} \end{pmatrix}$$

$$C \begin{pmatrix} \hat{U_D}^{p+1} \\ \hat{\zeta_D}^{p+1} \\ \hat{z_D}^{p+1} \end{pmatrix} = D \begin{pmatrix} \hat{U_D}^{p+\frac{1}{2}} \\ \hat{\zeta_D}^{p+\frac{1}{2}} \\ \hat{z_D}^{p+\frac{1}{2}} \end{pmatrix}$$

Where:

$$A = \begin{pmatrix} 1 & Cr \times i \sin\frac{1}{2} n & 0 \\ Cr \times i \sin\frac{1}{2} n & 1 + Fr \times Cr \times \frac{1 - e^{-in}}{2} & -Fr \times Cr \times \frac{1 - e^{-in}}{2} \\ 0 & 0 & 1 \end{pmatrix}$$

$$B = \begin{pmatrix} 1 - Fr \times Cr \times \frac{i \sin n}{2} & 0 & 0 \\ 0 & 1 & 0 \\ -\frac{1}{4} MF \times \psi \times Cr \times i(\sin\frac{1}{2} n + \sin\frac{3}{2} n) & 0 & 1 \end{pmatrix}$$

$$C = \begin{pmatrix} 1 + \frac{1}{4}Fr \times Cr \times (3 - 4e^{-in} + e^{-2in}) & 0 & 0 \\ 0 & 1 & 0 \\ 0 & 0 & 1 \end{pmatrix}$$

$$D = \begin{pmatrix} 1 & -Cr \times i \sin\frac{1}{2}n & 0 \\ -Cr \times i \sin\frac{1}{2}n & 1 - Fr \times Cr \times \frac{1-e^{-in}}{2} & Fr \times Cr \times \frac{1-e^{-in}}{2} \\ -\frac{1}{4}MF \times \psi \times Cr \times i(\sin\frac{1}{2}n + \sin\frac{3}{2}n) & 0 & 1 \end{pmatrix}$$

So:

$$\begin{pmatrix} \hat{U_D}^{p+1} \\ \hat{\zeta_D}^{p+1} \\ \hat{z_D}^{p+1} \end{pmatrix} = C^{-1}DA^{-1}B \begin{pmatrix} \hat{U_D}^{p} \\ \hat{\zeta_D}^{p} \\ \hat{z_D}^{p} \end{pmatrix}$$

4.3.3 Stability

A basic property that any acceptable discretization method must obtain is stability. A related phenomenon is instability. Usually, algorithms would approach the right solutions in the limit, if there is no rounding or truncation errors, but depend on the specific computational method, error may be magnified, leading to instability. Rewrite the above equations:

$$\varepsilon^{p+1} = G\varepsilon^{p} \tag{4.3}$$

Where G is the amplification matrix, $G = C^{-1}DA^{-1}B$. If S is a certain transformation which diagonalizes G, then Equation(4.3) becomes:

$$\begin{aligned} (S^{-1}\varepsilon^{p+1}) &= (S^{-1}GS)(S^{-1}\varepsilon^{p}) \\ or : \varepsilon'^{p+1} &= G'\varepsilon'^{p} \end{aligned} \tag{4.4}$$

where $\varepsilon' = S^{-1}\varepsilon$. G' is a diagonal matrix, where the values on the diagonal

are the eigenvalues of G:

$$G' = \begin{pmatrix} \varphi_1 & 0 & 0 \\ 0 & \varphi_2 & 0 \\ 0 & 0 & \varphi_3 \end{pmatrix}$$

The error at time level $p+1$ may be related to the error at time level 1 and by repeating the application of Equation(4.4).

$$\varepsilon'^{p+1} = G'\varepsilon'^{p} = (G')^2\varepsilon'^{p-1} = \ldots = (G')^p\varepsilon'^{1}$$

where:$(G')^p = \begin{pmatrix} \varphi_1^p & 0 & 0 \\ 0 & \varphi_2^p & 0 \\ 0 & 0 & \varphi_3^p \end{pmatrix}$

It follows from Equation(4.3.3) that if any of the eigenvalues of G lies outside the unit circle (i.e. $|\varphi| > 1$),then the original seed error ε'^1 will be amplified. The error eventually grows exponentially, increasing approximately as $|\varphi|^p_{max}$,where $|\varphi|_{max}$ is the eigenvalue of G with the greatest magnitude.

Law 1 *The time integration scheme is stable if the eigenvalues of the amplification matrix lie on or within the unit circle, i.e.*

$$|\varphi| \leq 1$$

Some typical values are chosen in Figure (4.2) and $MF \times \psi$ is equal to 10^{-5}. φ_1 and φ_2 are surface wave modes and φ_3 is bed wave mode. In this specific case, all the magnitude of the eigenvalues are smaller than one which proves the scheme is a stable. With increasing N, the magnitude goes to a steady solution nearly equal to one, which means the larger the grid size, the more numerical dispersion it is. The error analysis will be done later.

Figure (4.3) shows an unstable case, with ϕ_2 larger than one. The same Froude number and Courant number as the previous settings, but with larger Morfac and higher ψ.

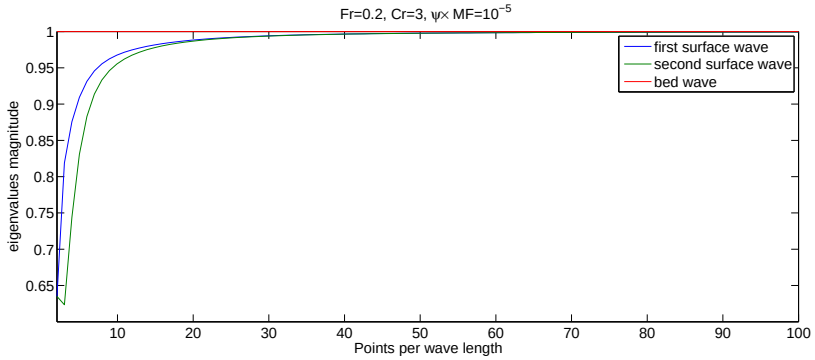

Figure 4.2: *A stable case, Fr=0.2, Cr=3,* $\psi \times MF = 10^{-5}$

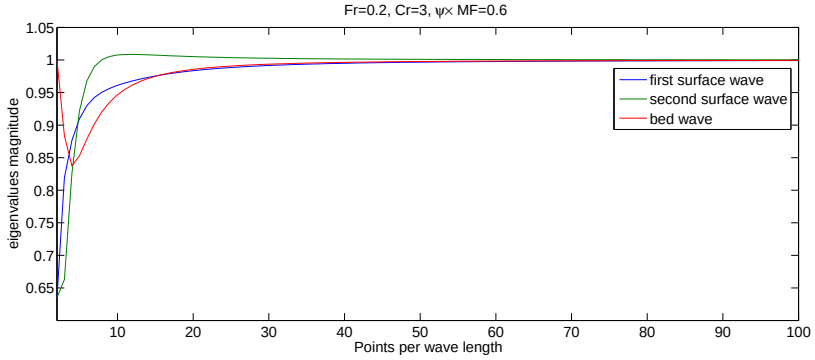

Figure 4.3: *An unstable case, Fr=0.2, Cr=3,* $\psi \times MF = 0.6$

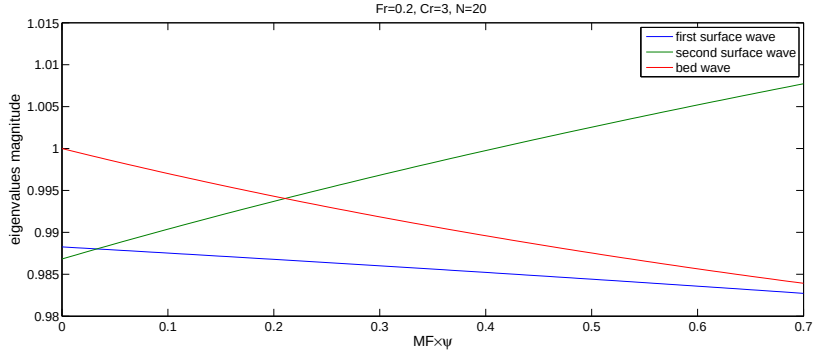

Figure 4.4: *Stability with increasing sediment transport*

Table 4.1: *Upper limit of MF×ψ for a stable model, N=8*

	cr=1	2	5	10
Fr=0.1	0.90	0.68	0.48	0.47
0.2	0.91	0.70	0.56	0.55
0.3	0.92	0.71	0.65	0.64
0.4	0.93	0.73	0.72	0.65
0.5	0.94	0.75	0.74	0.53
0.6	0.95	0.78	0.77	0.45

Table 4.2: *Upper limit of MF×ψ for a stable model, N=20*

	cr=1	2	5	10
Fr=0.1	0.70	0.52	0.29	0.18
0.2	0.69	0.52	0.30	0.20
0.3	0.69	0.51	0.31	0.22
0.4	0.68	0.51	0.31	0.23
0.5	0.67	0.50	0.31	0.24
0.6	0.67	0.50	0.31	0.24

Large Morfac combined with high sediment transport factor will cause instability in the numerical scheme. The product of MF and ψ should be smaller than 0.4 for this Froude number, Courant number and N, i.e.:

$$MF\psi \leq 0.4 \quad \text{for} \quad Fr = 0.2$$

See Figure (4.4). The amplification factor for the second surface wave will become larger than one, which means in the model, the hydrodynamic will first become unstable leading to a model crash. Compared with the stability criteria derived from the analytical model, we can see that the numerical schemes reduces the stability limits. Lower values of Morfac and ψ will cause instability compared to the analytical model.
As shown in Table (4.3), (4.2) and (4.1), large Courant number decrease

Table 4.3: *Upper limit of MF×ψ for a stable model, N=100*

	cr=1	2	5	10
Fr=0.1	0.67	0.50	0.29	0.17
0.2	0.66	0.49	0.28	0.17
0.3	0.65	0.49	0.28	0.17
0.4	0.64	0.49	0.28	0.17
0.5	0.64	0.49	0.28	0.16
0.6	0.63	0.46	0.28	0.16

the stability limits of the model, but the effect of Froude number is not significant. The effect of N is significant when N is small. When N increases from 8 to 20, the upper limit of $MF \times \psi$ decreases over 20%. N=8 is the most critical case to cover the courant number of 1 to 10 and N=20 is the most commonly used points per wavelength in practice. So Courant number is the most sensitive element in stability. A rough estimation can be made in advance, see Equation (4.5). It is based on N=100 case, which is the most unstable case. So it is a sufficient but not necessary criterion for a stable model.

$$MF \times \psi \times Cr^{0.6} \leq 0.63 \tag{4.5}$$

Stability with downwind bed level

As discussed in Section (4.3.1), in Delft3D model, a downwind scheme for the bed level could also be used. The final Matrix is changed:

$$A = \begin{pmatrix} 1 & Cr \times i \sin\frac{1}{2}n & 0 \\ Cr \times i \sin\frac{1}{2}n & 1 + Fr \times Cr \times \frac{e^{in}-1}{2} & -Fr \times Cr \times \frac{e^{in}-1}{2} \\ 0 & 0 & 1 \end{pmatrix}$$

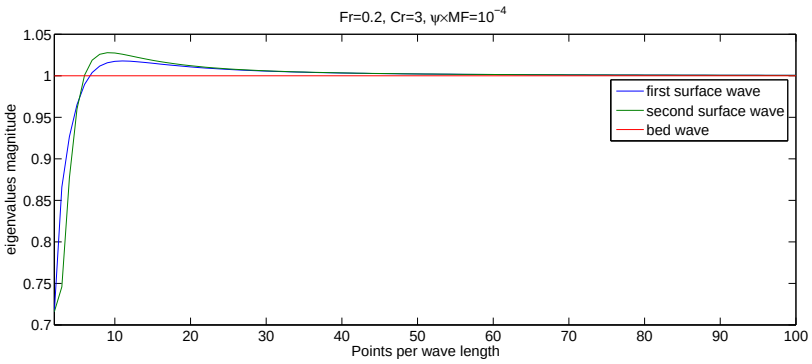

Figure 4.5: *An unstable model when using downwind scheme for bed level, Fr=0.2, Cr=3,* $MF \times \psi = 10^{-4}$

$$D = \begin{pmatrix} 1 & -Cr \times i \sin \frac{1}{2}n & 0 \\ -Cr \times i \sin \frac{1}{2}n & 1 - Fr \times Cr \times \frac{e^{in}-1}{2} & Fr \times Cr \times \frac{e^{in}-1}{2} \\ -\frac{1}{4}MF \times \psi \times Cr \times i(\sin \frac{1}{2}n + \sin \frac{3}{2}n) & 0 & 1 \end{pmatrix}$$

where B and C remain the same.

From Figure (4.5), the model becomes unstable even for $MF \times \psi$ is quite small.

Consequently, in practice, the reason for the instability of a decreasing water depth and increasing water depth is different. The previous one can be caused by the downwind scheme and the later one by the real Morfac instability.

Stability with explicit scheme for water depth

In Delft3D, the water depth in the continuity equation is not taken fully implicitly during the beginning of the computation. So now the explicit scheme for the water depth is investigated.

If we compared Table (4.4) and (4.2), we can see that the upper limit of $MF \times \psi$ is decreased in the high Froude number and high Courant number region.

Table 4.4: *Upper limit of MF×ψ for a stable model for explicit water depth, N=20*

	cr=1	2	5	10
Fr=0.1	0.70	0.53	0.30	0.18
0.2	0.69	0.52	0.30	0.17
0.3	0.69	0.51	0.29	0.17
0.4	0.68	0.51	0.29	0.17
0.5	0.67	0.50	0.28	0.16
0.6	0.67	0.49	0.18	0.16

Though Equation (4.5) is a sufficient criterion, we expect the stability will be worse in Delft3D for all the non-transparent errors included.

4.4 Error Analysis

Two related errors can be derived: celerity error and amplitude error from the von-Neuman analysis. According to Equation (4.3), if the initial condition is assumed to have a form like:

$$\varepsilon'^{0} = \varepsilon_0' e^{ik_D x_D}$$

So the complete time-dependent solution is:

$$\varepsilon'^{p+1} = \varepsilon_0' |G'^{p}| e^{ik_D x_D} = \varepsilon'^{0} |G'^{t/\Delta t}| e^{ik_D x_D} = \varepsilon_0' e^{\ln(|G|t/\Delta t) + ik_D x_D}$$

Similar to the analytical model, now the real part of $\ln|G|$ is the amplification information and the imaginary part is celerity. The same criteria is used as in the analytical model. (See Equation (3.24) to (3.25)). Now, $a = \Im \ln|G|$ and $b = \Re \ln|G|$.

There is not only Morfac induced errors, but also numerical errors. If numerical errors are assumed to be neglected for large N and small Courant number, the classification is defined in Table 4.5.

Table 4.5: *Morfac error and Numerical error,* $\psi = 10^{-6}$

Case	ψ	Morfac	N	Courant	Error
1	10^{-6}	1	10000	0.0001	Negligible error
2	10^{-6}	100	10000	0.0001	Morfac error
3	10^{-6}	1	20	3	Numerical error
4	10^{-6}	100	20	3	Morfac error+Numerical error
5	10^{-6}	100	10	3	Morfac error+Numerical error(N)
6	10^{-6}	100	20	6	Morfac error+Numerical error (Cr)

First, the eigenvalues of Case 1 are used to compare with the analytical solutions.

From Figure (4.6) and (4.7), we can see that though the Courant number is small and N is large, the numerical approximations still have effects to the solutions. The difference in celerity and bed wave amplitude is quite small or maybe even due to the machine precision. However, the amplitude difference in surface waves is relatively large and it increases with Froude number. This is caused by the spatial discritization of the advection term in momentum equations which adds numerical dissipation on the surface and it will increases with Froude number.

Ideally, Case 1 should be the benchmark for other cases. But since we are more interested in the Morfac effect, Case 3 is a better benchmark than Case 1 due to the effect of initial numerical errors are included. As a result, first, we are going to the compare the Morfac error alone and numerical error alone. Case 1 is the benchmark. Then, Case 3 is setup as benchmark to further study the coupling effect of Courant number and N.

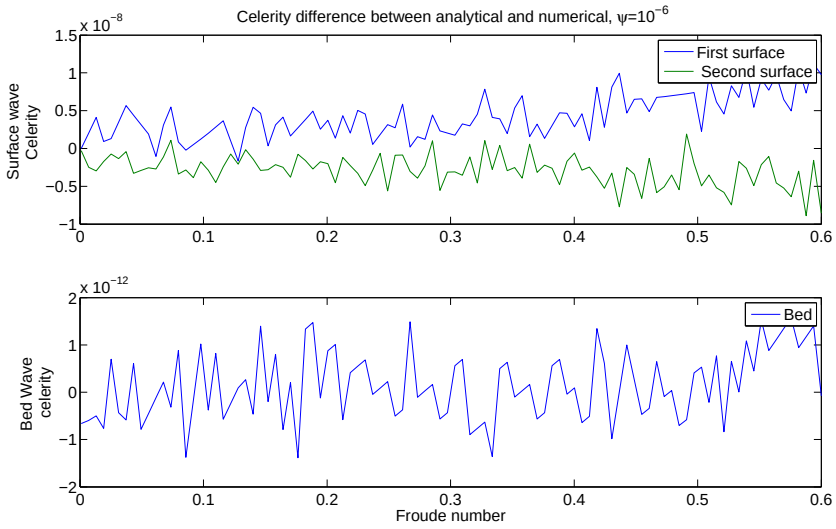

Figure 4.6: *Celerity difference between analytical solution and numerical solution,N=10000, Cr=0.0001,* $MF \times \psi = 10^{-6}$

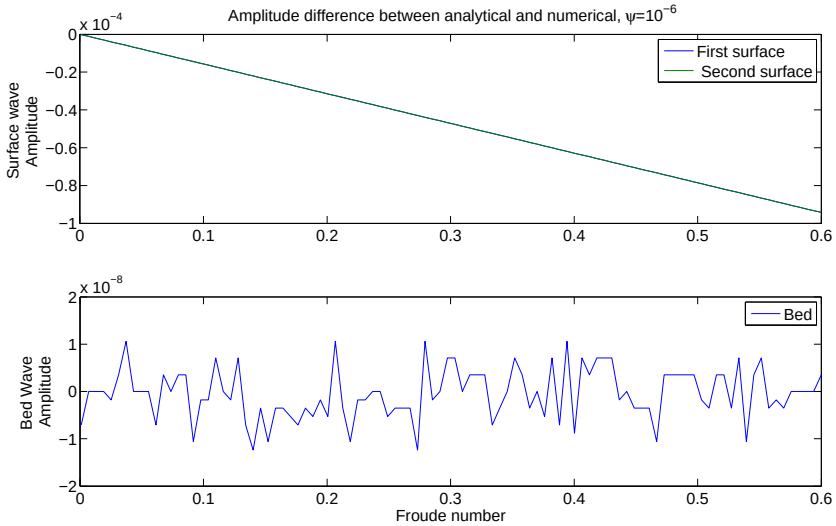

Figure 4.7: *Amplitude difference between analytical solution and numerical solution,N=10000, Cr=0.0001,* $MF \times \psi = 10^{-6}$

Comparison of Morfac error and Numerical error alone

From the analytical model, we see that Morfac does affect the amplitude and celerity of the model if friction is included. So first, a comparison of Morfac error and numerical error is done to investigate which error has a larger magnitude.

Case 2 and 3 are studied using Case 1 as the benchmark.

The shallow water equation when friction is absent is a purely hyperbolic equation, by definition, is free of dissipation. But the equation is solved numerically, which may reduce the amplitude and change the shape of the initial wave in a way analogous to a diffusion process, the method is said to contain dissipation. The error is not induced by Morfac alone, numerical approximations also have strong effect.

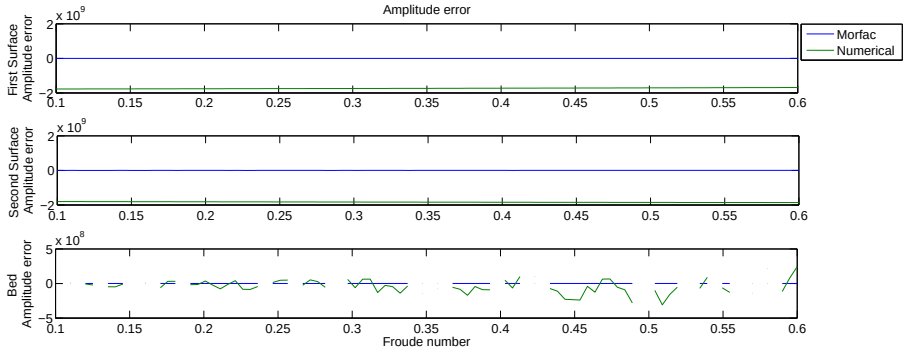

Figure 4.8: *Morfac (Case 2) and Numerical (Case 3) induced amplitude error*

In Figure (4.8), the amplitude error for case 2, 3 and 6 are studied. Case 1 is set up as the bench mark. And due to the scale of the axis, the total error overlaps with the numerical errors.We can see that the Morfac induced amplitude error is so small compared to the numerical induced error. The same phenomenon is shown in the celerity. See Figure (4.9). The numerical implementation damps out the amplitude and shows a leading phase error in both the surface and bed.

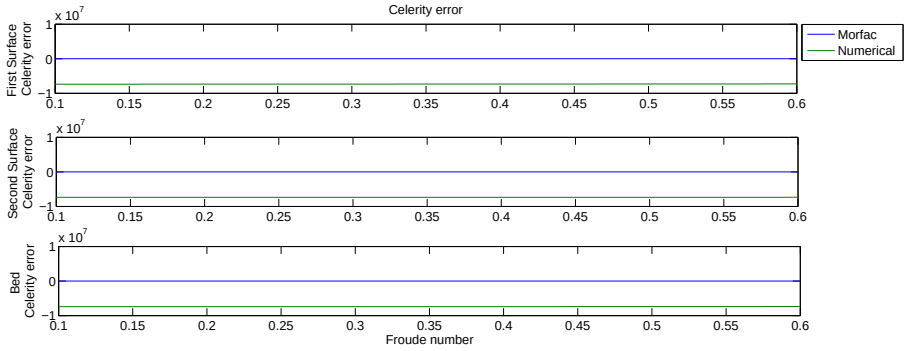

Figure 4.9: *Morfac (Case 2) and Numerical (Case 3) induced celerity error*

Combined effect

Case 4, 5 and 6 are going to studied here based on the benchmark of Case 3 where the numerical errors are accepted.

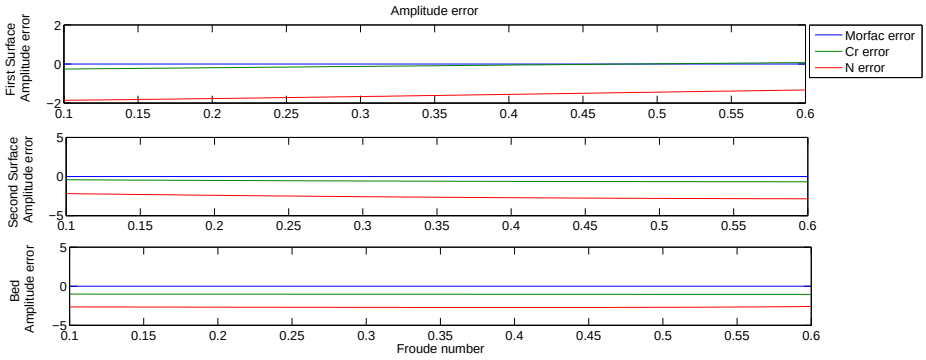

Figure 4.10: *Morfac (Case 4),Courant (Case 5) and N (Case 6) induced amplitude error*

In Figure (4.10), the amplitude error induced by Morfac is small compared with larger Courant number and smaller N. Moreover, if N is halved, and Courant number is doubled, N will induce more amplitude errors than Courant number.

The same phenomenon we can see for the celerity. In Figure (4.11), the celerity error induced by Morfac is also small compared with larger Courant number and smaller N. But N and Courant number will have same effect to the celerity.

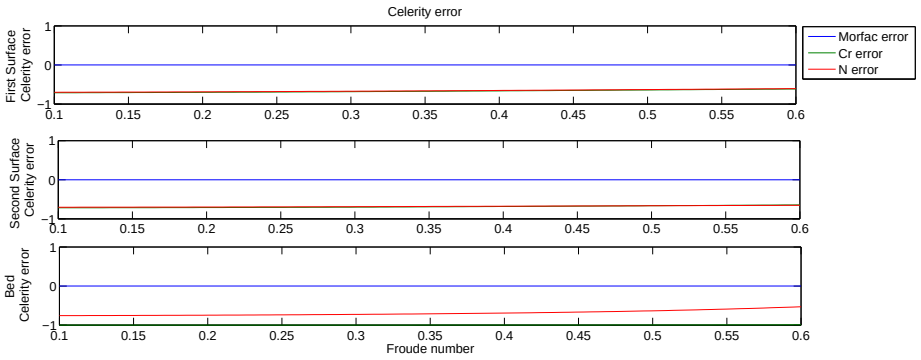

Figure 4.11: *Morfac (Case 4),Courant (Case 5) and N (Case 6) induced celerity error*

4.4.1 Detailed analysis of Morfac effect

For the Morfac induced error is so small to see compared to numerical changes. Case 4 is studied alone.

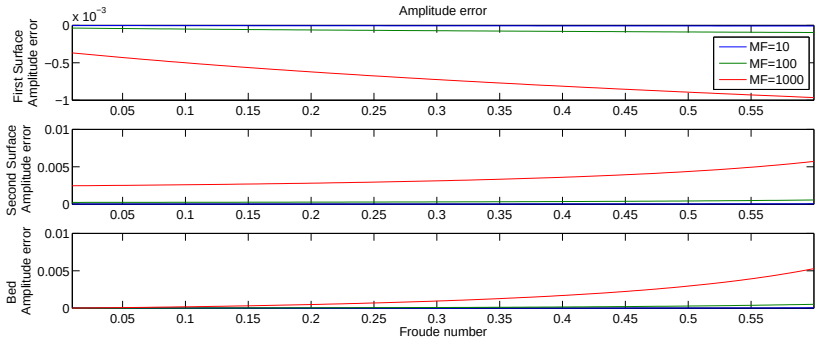

Figure 4.12: *Morfac (Case 4) induced amplitude error,* $\psi = 10^{-6}$

First, the amplitude is investigated. From Figure (4.12), we can see that Morfac will underestimate the amplitude of the first surface wave, but overestimate both the second surface wave and the bed wave. Normally, the second surface wave has the largest error.

In Figure (4.13), the Morfac induced celerity error is investigated. A leading phase error is shown in the first surface wave and bed wave while the second surface wave has a leading phase error.

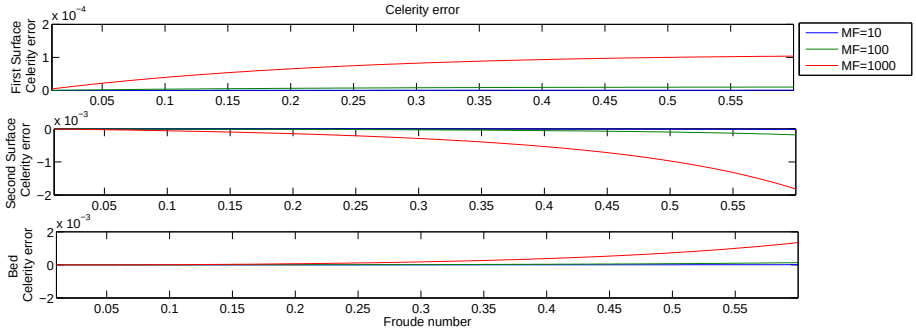

Figure 4.13: *Morfac (Case 4) induced celerity error,* $\psi = 10^{-6}$

Table 4.6: *Summary of errors*

	Numerics	Morfac
φ_1,amplitude	underestimate	underestimate
φ_2,amplitude	underestimate	overestimate
φ_3,amplitude	underestimate	overestimate
φ_1,phase	leading	lagging
φ_2,phase	leading	leading
φ_3,phase	leading	lagging

Brief Summary

To both celerity and amplitude, the value of the numerical error is much larger than that of Morfac error for $MF = 100$. But the basic behavior is changed by Morfac. See Table (4.6).

4.4.2 Critical Morfac

Firstly, the critical Morfac is studied based on the total error which is the sum of celerity and amplitude error, see Equation (3.22). If either of the three waves exceed 1 % of error, then the value of the Morfac is the critical Morfac. The benchmark is setup as Case 3, i.e., initial numerical errors are accepted.

Figure 4.14 shows the relation between critical Morfac and ψ. A similar

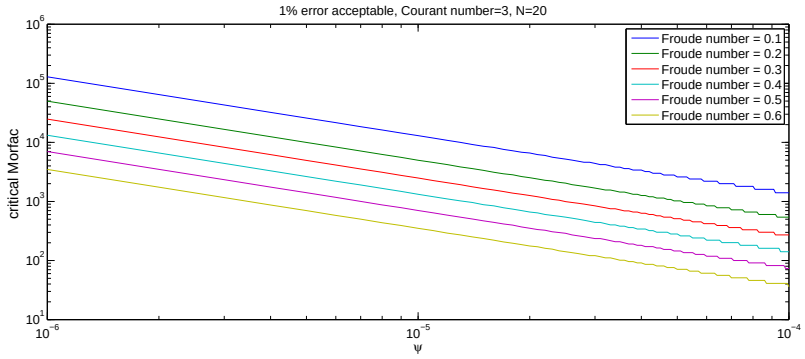

Figure 4.14: *Critical morfac based on total error with N=20, Courant number=3*

Table 4.7: *Upper limit of $MF\psi$ with different Courant number and N*

	Cr=3, N=20	Cr=3, N=10	Cr=6, N=20
Fr=0.1	0.1312	0.126	0.122
Fr=0.2	0.06	0.046	0.046
Fr=0.3	0.03	0.02	0.022
Fr=0.4	0.014	0.01	0.01
Fr=0.5	0.007	0.005	0.006
Fr=0.6	0.004	0.002	0.003

trend is shown in the analytical model. Points per wavelength and Courant number is chosen to be the most frequent used values in practice.

Table (4.7) shows the upper limit of $MF \times \psi$ with different Courant number and N. We can see that small N and large Courant number will have low upper limit value.

If amplitude is more of focused, then the accumulated amplitude error after one wavelength can be used. And the typical wavelength is specified. If a small scale is used, $\lambda_T = 100m$. Figure (4.15)shows a much larger critical Morfac than total error shows.

Compared Table (4.8) and (3.4), larger critical Morfac is derived. The main reason is friction term is not included in the model. And as concluded previously, friction term is not good for accuracy.

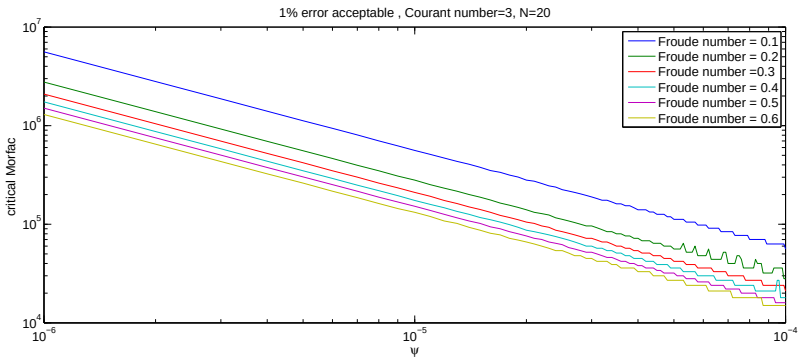

Figure 4.15: *Critical morfac based on accumulated amplitude error after one wavelength, N=20, Courant number=3*

Table 4.8: *Critical Morfac in the numerical model for different situations, N=20, Courant number=3*

	Froude number	ψ	Morfac
Wadden Sea	0.3	10^{-5}	4000
Western Scheldt	0.4	3×10^{-5}	3000
North Sea	0.1	10^{-6}	10000

The effect of dimension parameters

Dimensionless parameters are studied before, but in practical, it is not so convenient to use dimensionless parameters. Usually, during the model setup, dimension parameters are used, like the flow velocity, grid size, time step etc. In order to make the results more transparent, water depth and morphological scale is specified. Then Froude number and ψ is converted into velocity, points per wave length into grid size, and Courant number into time step.

In Figure (4.16), we can see that large velocity and time step, or grid size will all reduce the critical Morfac. Large velocity means large Froude number and ψ which all cause small critical Morfac. It has a dominant

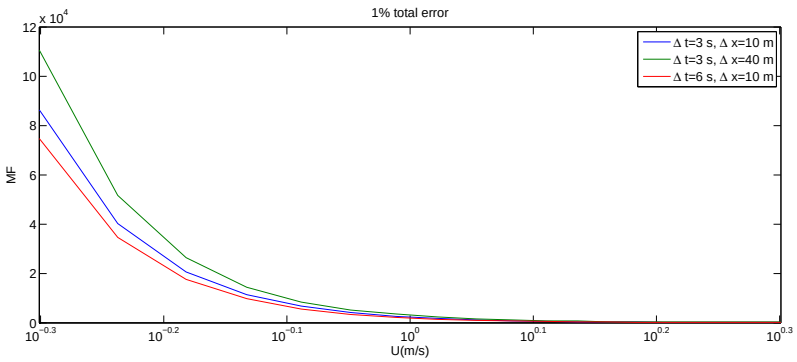

Figure 4.16: *Critical Morfac with Flow velocity, h(water depth)=4m, λ_T=200m*

effect, when flow velocity is really low, the maximum Morfac can up to hundred thousand, but when flow velocity increases to 2 m/s, the critical Morfac can only be around thousand. Large time step can be translated to large Courant number when only time step is adjusted. Larger Courant number will also induce large errors. The effect of grid size will change both the Courant number and N. Larger grid size leads to smaller N which should reduce the model accuracy while larger grid size also leads to smaller Courant number, on the other hand, which should increase the accuracy. In Figure (4.16), large grid size will improve the accuracy. As long as the initial numerical error is acceptable, coarse grid is preferred.

4.5 Comparison of analytical and numerical model

In the analytical model, the controlled parameters are Froude number, ψ, and friction if it is included. In the numerical model, the systems become even more complicated since points per wavelength N and courant number are also included. The effect of the ψ, and Froude number to error analysis and critical Morfac is similar in the physical model and numerical model. In the analytical model, there exists only Morfac error which is always dominant in the system. But in the numerical model, the numerical scheme has large effect to both the accuracy and stability. Compared with

Table 4.9: *Comparison of the sufficient criteria for $MF\psi$ in analytical and numerical model ($N \leq 100, Cr \leq 10, Fr \leq 0.6$*

	Analytical	Numerical
Stability	$MF\psi \leq 1$	$MF\psi \times Cr^{0.6} \leq 0.63$
Accuracy	$MF\psi \leq 0.06$	$MF\psi \leq 0.003$

the order of error induce by the numerics and Morfac, numerical errors are usually far larger than Morfac errors alone. Most importantly, they are not independent. The introduction of Morfac may change the basic behavior. The model properties also affect the accuracy and stability. Small N will have more numerical damping, so the model is more stable than large N. But on the other hand, in the accuracy analysis, small N will have more errors than large N in the same case. Large Courant number will both make the more unstable and more inaccurate.
A sufficient criteria for $MF \times \psi$ is listed for both analytical and numerical model in Table (4.9). But the accuracy of the numerical model also depends on the Courant number and N, which the relationship is unknown.

4.6 Conclusion

1. Large Courant number , N and $MF\psi$ will all induce instability of the numerical model.

2. Numerical error on the surface wave is far larger than the Morfac error. The bed wave will show an overestimate of amplitude and a lagging phase.

3. In the accuracy analysis, large Froude number and Courant number and small N will have lower upper limit of $MF\psi$

Chapter 5

Analysis of Morfac in Delft3D Model

5.1 Introduction

5.1.1 Aim

The fundamental behavior of the Morfac concept in an analytical and numerical model of 1D unidirectional flow has been investigated in the previous chapters. Some basic conclusions have been derived:

1. Morfac does aggravate the instability of the model. For the stability criteria derived previously, if the product of $MF \times \psi$ is extremely large. For a Froude number of 0.2 and Courant number of 4, the upper limit of $MF \times \psi$ is 0.35. But we expect in the Delft3D model, the value will decrease because of the limitation of the analysis. For instance: the downwind bed level or the explicit water depth and etc.

2. Morfac will change the surface wave (hydrodynamics). The second surface wave which propagates in the opposite flow direction will first show unrealistic amplitude when $MF \times \psi$ is large.

3. The dimensionless parameters: Froude number and sediment transport factor ψ play an important role. But it is much easier to

look at the dimensional parameters instead. The larger the flow velocity and time step, the larger the error. The smaller the grid size, the larger the error.

In order to verify the above findings, test runs in Delft3D are done.

5.1.2 Approach

A 1D small perturbation analysis is done in the Delft3D model.The following tests are run to investigate the effect of Morfac and the parameters. The model can be classified as a small morphological scale. Though the Chézy friction coefficient is constant in the model, the friction term also strongly depends on the flow velocity. The larger the flow velocity, the stronger the effect of friction will be.
Hydrodynamic and morphological settings for the base case:

Domain length	9km
Ambient water depth	4m
Height of disturbance	20cm
Wavelength of perturbation	200m
Flow velocity	1.25m/s
Grid size	10m
Time step	6s
Simulation period	30 days
Chezy coefficient	65 $m^{1/2}/s$
Upstream flow boundaries	Discharge
Upstream sediment transport boundaries	0
Downstream flow boundaries	Water level
Downstream sediment transport boundaries	0
d_{50}	$350\mu m$
Sediment Formula	Engelund Hansen

The dimensionless values is calculated at the equilibrium slope not at the perturbation:

Froude number	$\frac{U}{\sqrt{gh}} \approx 0.2$
ψ	$5 \times \frac{2.6\times10^{-5}U^5}{Uh} \approx 8 \times 10^{-5}$
Points per wave length	$\frac{\lambda_T}{\Delta x} = 20$
Courant number	$\frac{\sqrt{(gh)}\Delta t}{\Delta x} \approx 4$
Friction parameter	$\frac{g\lambda_T}{C^2h} \approx 0.1$

Table 5.1: *Test cases of Delft3D*

Test parameters	Value	Test Morfac
Flow velocity (m/s)	1.25,1.88,2.50	1,8,128,1024
$\Delta x(m)$	10,5,2.5	1,8,128,1024
$\Delta t(s)$	6,12,3	1,8,128,1024

The values of Morfac is chosen to be a multiple of 2 in order to make the morphological time easy to compare. Flow velocity, time step and grid size is also changing to verify the effect to Morfac induced errors. And in order to verify the upper limit of Morfac, a high flow velocity is used. See all the test cases in Table (5.1). For the initial conditions see Figure (5.1).

5.2 Small perturbation analysis

5.2.1 Stability

Stability is also a kind of accuracy problem in a much larger scale. When instability of the model is shown, then all the accuracy of the model results are far away from reasonable.

First of all, the stability problem when applying Morfac is going to be investigated. From Figure (5.2), we can see a wave with unrealistic amplitude first appear on the water level.

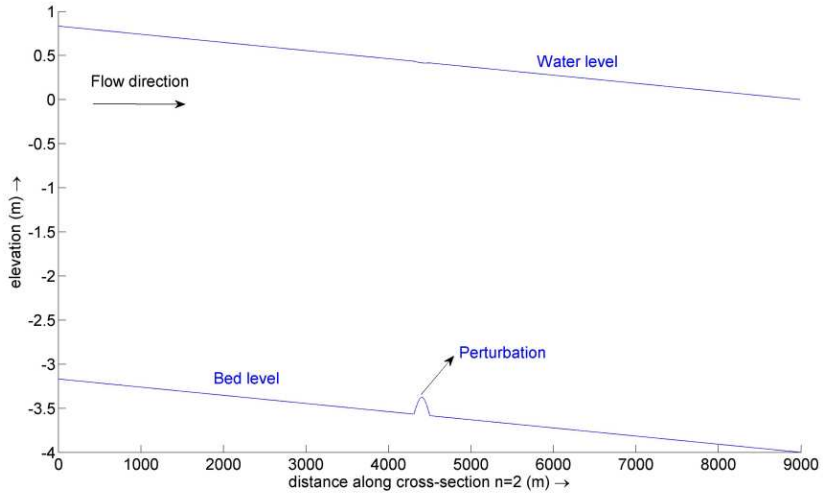

Figure 5.1: *Initial conditions for small perturbation analysis*

In Chapter 4, the stability of the numerical scheme similar to Defl t3D was studied. It was concluded that large values of $\psi \times MF$ will induce instability first on the surface wave which propagates opposite the flow direction. Hence the behavior observed in Delft3D agrees with the numerical analysis. In this particular case, ψ can be calculated by its physical meaning:

$$\psi = 5 \times \frac{S}{Q} = 5 \times \frac{2.6 \times 10^{-4}}{1.25 \times 4} = 2.6 \times 10^{-4}$$

$$MF \times \psi = 1024 \times 2.6 \times 10^{-4} \approx 0.26$$

This ψ is the maximum value which happens at the tip of the perturbation with the corresponding Froude number equal to 0.35.

Compared with the criteria derived in the numerical model, a Froude number of 0.35 and Courant number of 4, the upper limit of $MF \times \psi$ is 0.33. As we expected, the upper limit in Delft3D will decrease because of the difference in the numerical schemes we studied. The first guess is the downwind scheme for the bed level at the velocity point. From Figure (5.3), the instability of the total sediment transport is shown for a Morfac

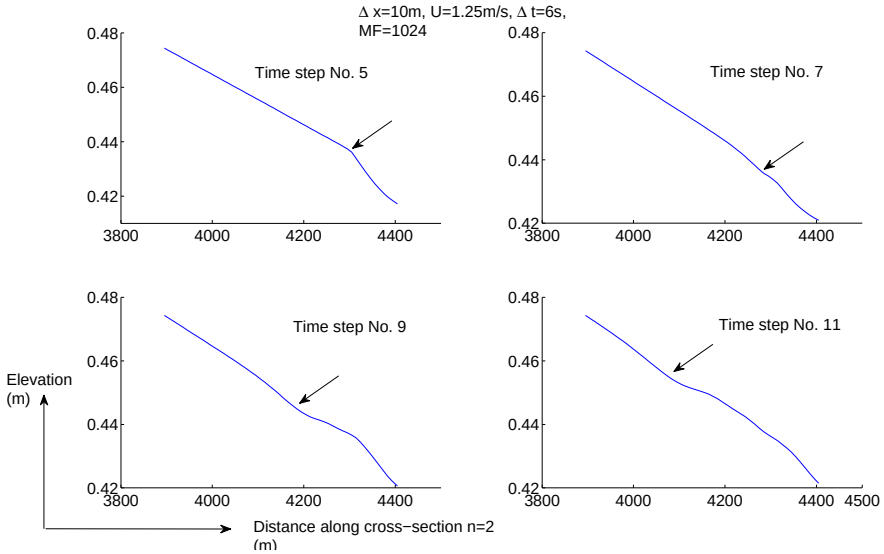

Figure 5.2: *Second surface wave in the opposite flow direction, $MF \times \psi$=0.26, Fr=0.2*

of 1024 with flow velocity equals to 1.25 m/s. At time step 2, there is a small variation of total sediment transport at the foot of the hump, and they will propagate in both directions. But at time step 14, the variation at the back foot damps out for the upwind scheme while the variation at the front becomes unstable for the downwind scheme.

Of course, there are other possibilities why the upper limit is decreased in the Delft3D model. In our previous analysis, only the internal scheme is investigated, so boundary could also contribute to the instability.

Due to the different algorithms applied between the internal and boundary, there is always a discontinuity of the values (like the total sediment transport) though it is low. See Figure (5.4). But with large Morfac, the difference could also be large.

Variable coefficient or non-linear effect could also cause instabilities, further investigation is needed. So the stability criteria for numerical scheme should be on top of the Delft3D model. Equation (4.5) still serves as a necessary criterion for the Delft3D model. Some models done by

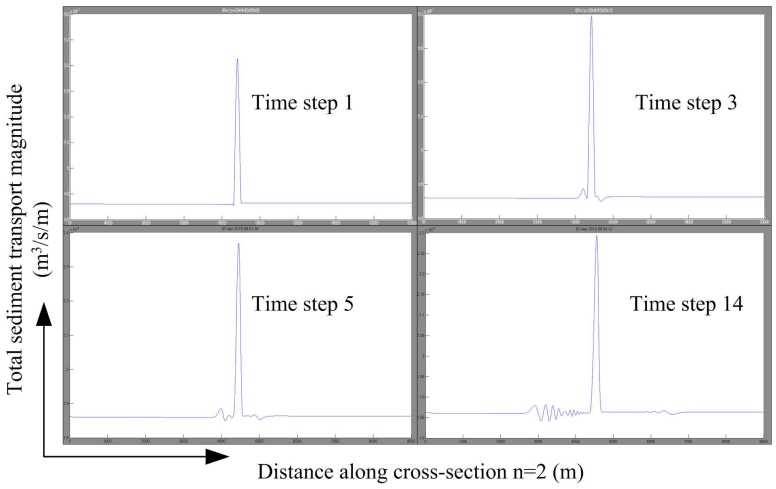

Figure 5.3: *Total sediment transport instability at the front of the hump,* $MF \times \psi = 0.26, Fr = 0.2$

C.M.Swinkels are also investigated to verify this criterion. See the model details in C.M.Swinkels [1].

The Courant number for Figure (5.5) is around 2.5, so if the model is stable, the product of $MF \times \psi$ is smaller than 0.5.

5.2.2 Effect of Morfac on the hydrodynamic

The hydrodynamic system is a feedback system, consisting of many elements, like the water level, flow velocity, sediment transport and so on. Morfac not only accelerates the bed mode but also affects the surface mode.

All the errors are compared at the same morphological time step. The hydrodynamic has become quasi-steady before the morphological change took place. Figure (5.6), the velocity difference compared with the Morfac equals to one is shown. At first, near the pit of the perturbation, there exists an error which is caused by the perturbation. And this error will propagate in both opposite or same as the flow direction. As Figure (5.6) shows, with large Morfac, the error in the opposite flow direction will be

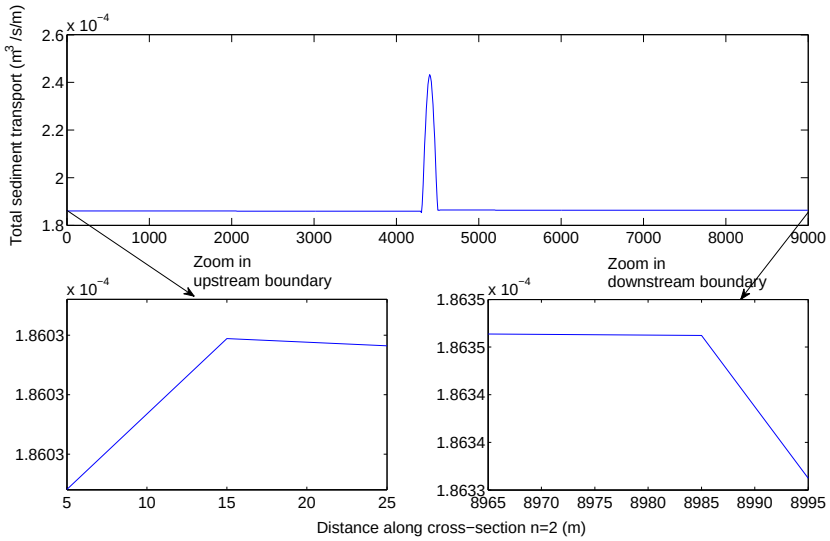

Figure 5.4: *Inaccurate boundary in Delft3D*

increased, and a larger area is disturbed which crashes the model. This behavior agrees with the stability criteria discussed before.

The error increases with time and the value of Morfac. The basic error phenomenon is the same as shown in the analytical and numerical model. For simplicity, only the largest relative error in the domain is shown in the table.

Table 5.2: *Computed maximum relative velocity error for U=1.25m/s,* $\Delta x = 10m, \Delta t = 6s, \psi = 2 \times 10^{-4}$

Morfac	Maximum Velocity error (after 5% wavelength)	Maximum Velocity error (after one wavelength)
8	1.47×10^{-5}	3.07×10^{-5}
128	2.68×10^{-4}	5.54×10^{-4}
1024	3.3×10^{-3}	4.6×10^{-3}

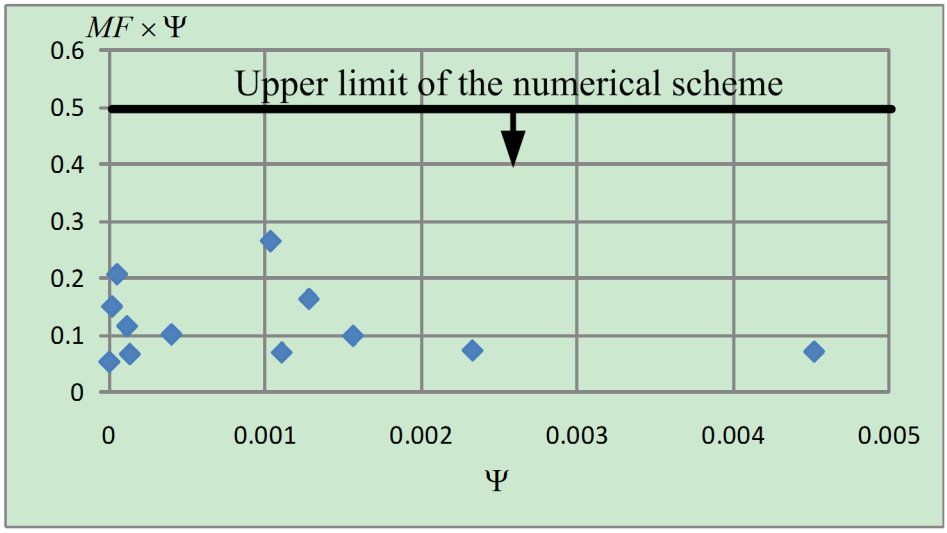

Figure 5.5: *Upper limit of $MF \times \psi$ in Delft3D model*

5.2.3 Effect of Morfac on the Morphology

Two elements are going to be investigated, one is the total transport and the bed level. The Engelund-Hansen sediment transport formula is used, total transport is all regarded as bed load. The total transport is a power function of velocity only. The error in Figure (5.7) shows a similar pattern as the velocity filed. But because the transport is a power of velocity, the transport error is much larger than the velocity error.

The bed level is the most interesting field related to morphology, the error is shown in Figure (5.8) and Table (5.3). The bed level error has the same order of magnitude as the depth-averaged velocity error and the largest error is around the area where the perturbation is situated.

5.2.4 The effect of flow velocity

As in the analytical and numerical models, it was found that ψ and Froude number are dominant factors when Morfac is tested, and they are both a function of the flow velocity. So if the sediment transport formula and the water depth in Delft3D model is kept unchanged, the flow velocity should

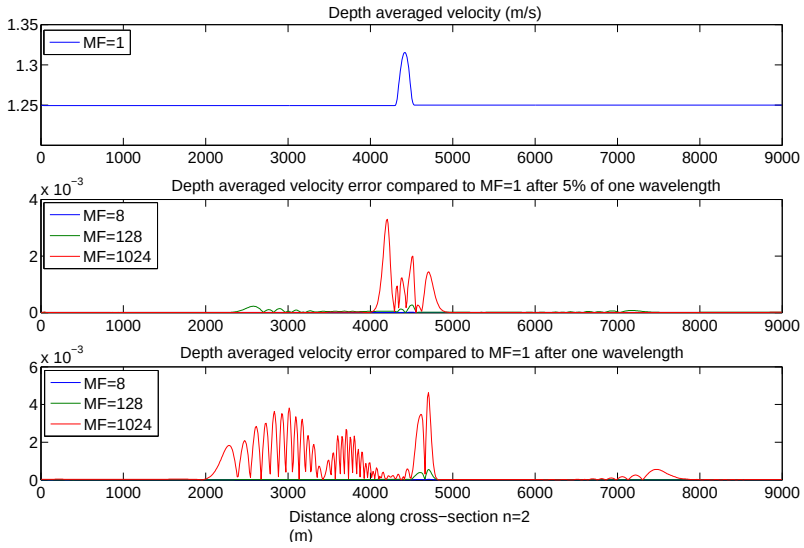

Figure 5.6: *Depth averaged velocity relative error, U=1.25m/s,* $\Delta x = 10m, \Delta t = 6s, \psi = 2 \times 10^{-4}$

Table 5.3: *Computed maximum relative bed level error for U=1.25m/s,* $\Delta x = 10m, \Delta t = 6s, \psi = 2 \times 10^{-4}$

Morfac	Maximum bed level error (after 5% wavelength)	Maximum bed level error (after one wavelength)
8	8.00×10^{-6}	2.92×10^{-5}
128	1.47×10^{-4}	5.32×10^{-4}
1024	1.5×10^{-3}	4.7×10^{-3}

show a strong effect on Morfac induced errors. The larger the velocity, the larger the Froude number and ψ. And $MF \times \psi$ is a criteria for stability, as ψ increases, the Morfac intuitively decreases. When $U = 1.25$m/s, a Morfac of 1024 will cause instability, but when velocity increases to 1.88m/s, a Morfac of 128 will crash the model. Moreover, if $U = 2.5$m/s, only a Morfac of 8 can keep the model stable.

The bed level error is investigated based the perturbation amplitude change after one wavelength.

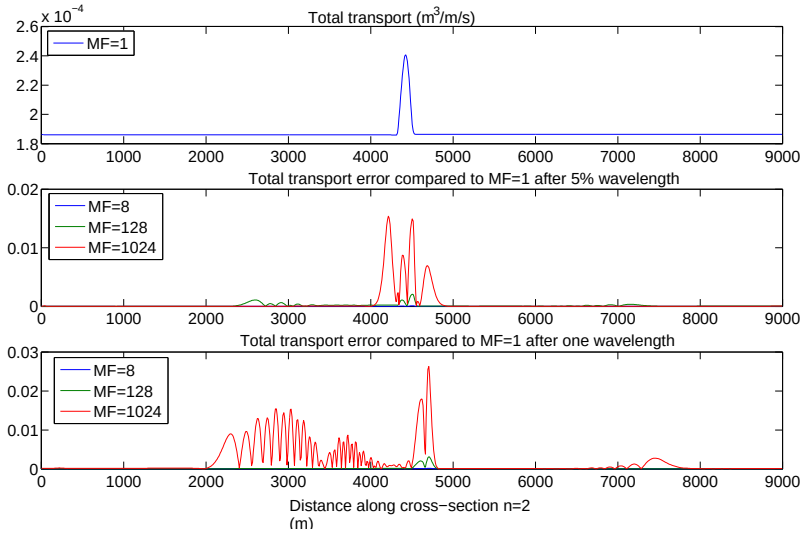

Figure 5.7: *Sediment transport relative error,U=1.25m/s,* $\Delta x = 10m, \Delta t = 6s, \psi = 2 \times 10^{-4}$

Morfac	Error(U=1.25m/s)	Error(U=1.88m/s)	Error(U=2.5m/s)
8	2.92×10^{-5}	3.32×10^{-5}	0.002
128	5.32×10^{-4}	0.0056	289.92
1024	4.7×10^{-3}	0.3764	2617

Table 5.4: *Bed level amplitude error after one wavelength for different velocities with corresponding Froude number of 0.2, 0.3 and 0.4,* $\Delta x = 10m, \Delta t = 6s$

Large error is shown for flow velocity equals to 2.5m/s, even when Morfac is small. So flow velocity is a dominant effect in the Morfac analysis.

5.2.5 The effect of grid size

Computational time is very sensitive to grid size, therefore in practise, lower grid size resolution is preferred as long as it gives reasonable errors. In previous chapters, the grid size is related to points per wavelength of the perturbation and Courant number. for large grid size will lead to less points per wavelength and lower courant number if Δt is fixed. The larger the grid size, the larger the numerical damping it induces. So the model

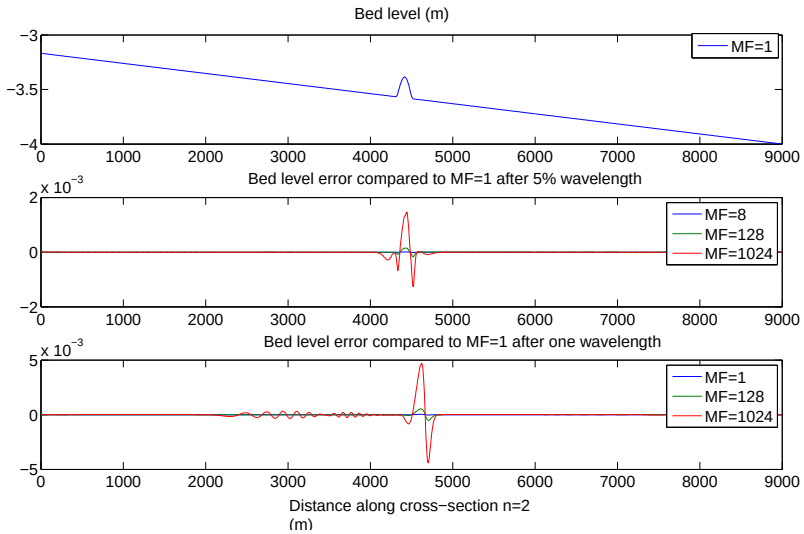

Figure 5.8: *Bed level relative error, U=1.25m/s,* $\Delta x = 10m, \Delta t = 6s, \psi = 2{\times}10^{-4}$

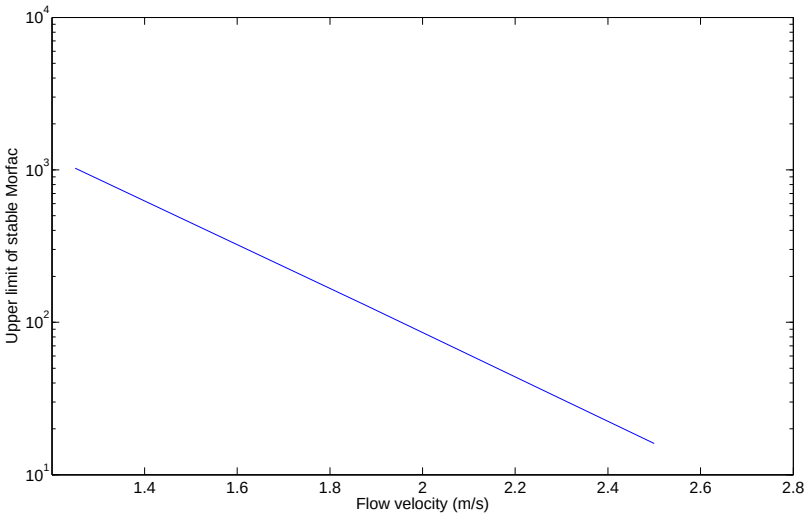

Figure 5.9: *Upper limit of a stable Morfac with flow velocity,* $\Delta x = 10m, \Delta t = 6s$

will be stable even for a larger Morfac but the model will not give any accurate results any more.

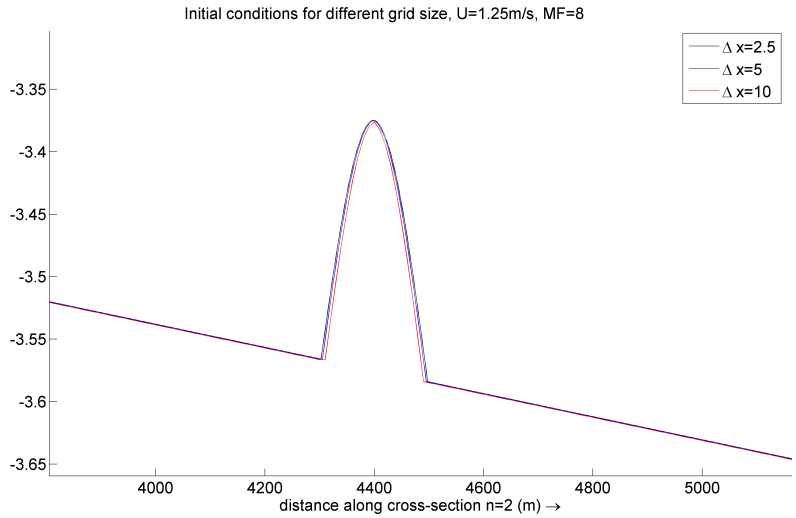

Figure 5.10: *Initial conditions for different grid size, U=1.25m/s,* $\Delta t = 3s$

As shown in Figure (5.10), even the initial conditions are not the same for different grid size. The larger the grid size, the smaller the amplitude of the perturbation is. The width of the perturbation is also not exactly the same. The smaller the grid size, the larger the width of the perturbation. These are all numerical errors.

In Figure (5.11), after one wavelength, the amplitude difference is significant for different grid size. It shows a nearly 20% error between the largest and the smallest grid size. Coarser grid will have more damping, in another word, coarse grid will have a more stable model, but also lead to a loss of accuracy.

In Table (5.5), the bench mark is setup as Morfac equals to one case. From Figure (4.16) in the previous chapter, we can see the effect of changing the grid size larger can give smaller errors. So if the numerical damping caused by large grid is acceptable, then large grid is preferred, for both stability and amplitude accuracy reason.

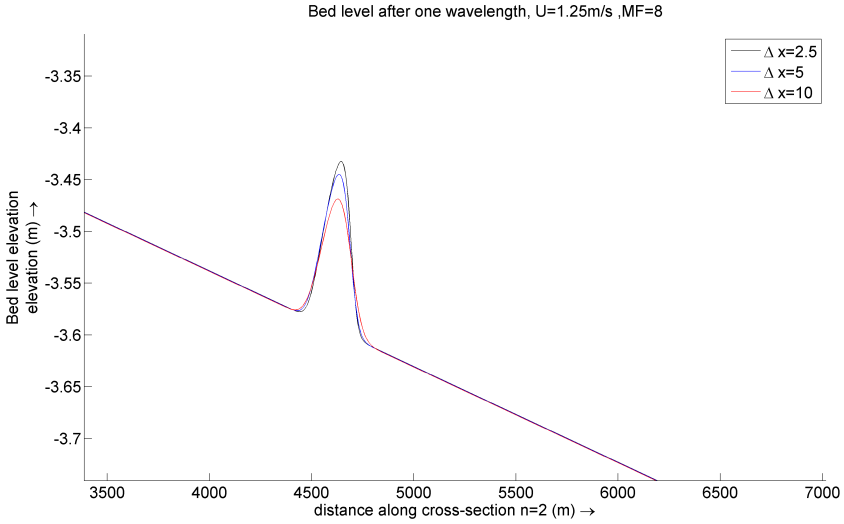

Figure 5.11: *Bed level after one wavelength for different grid size, U=1.25m/s,*$\Delta t = 3s, \psi = 2 \times 10^{-4}$

Morfac	$\Delta x = 10m$	$\Delta x = 5m$	$\Delta x = 2.5m$
8	2.92×10^{-5}	4.12×10^{-5}	5.13×10^{-5}
128	5.32×10^{-4}	7.62×10^{-4}	9.56×10^{-4}
1024	4.7×10^{-3}	7.4×10^{-3}	2.06

Table 5.5: *Bed level amplitude error for different grid size after one wavelength, U=1.25m/s,* $\Delta t = 6s, \psi = 2 \times 10^{-4}$

Morfac	$\Delta t = 3s$	$\Delta t = 6s$	$\Delta t = 1.5s$
8	2.92×10^{-5}	5.44×10^{-5}	2.01×10^{-5}
128	5.32×10^{-4}	1×10^{-3}	3.63×10^{-4}
1024	4.7×10^{-3}	0.011	0.0028

Table 5.6: *Bed level amplitude error for different time step after one wavelength,U=1.25m/s,* $\Delta x = 10m, \psi = 2 \times 10^{-4}$

5.2.6 The effect of time step

Large time steps can decrease the total simulation time dramatically, on the other hand, it leads to larger errors.

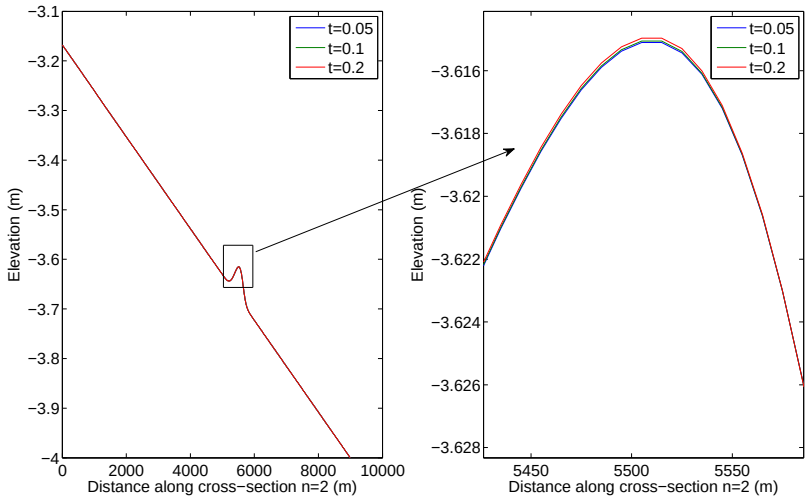

Figure 5.12: *The effect of time step after one wavelength for U=1.25m/s,* $\Delta x = 10m, \psi = 2 \times 10^{-4}$

In Figure (5.12), little difference is shown for different time steps. Only through detailed zoom in, we can see small time steps have more damping than large time steps. Detailed error is shown in Table (5.6).

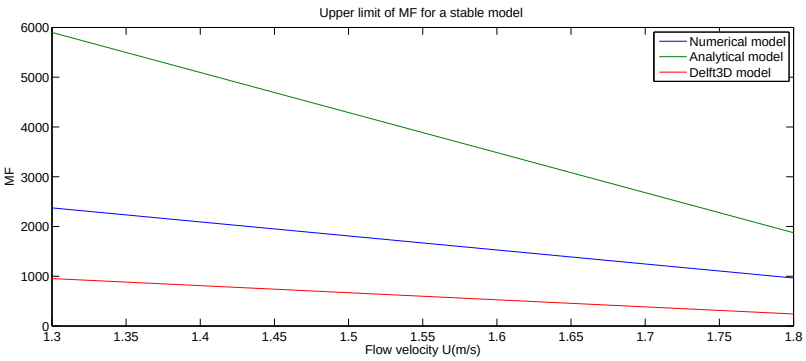

Figure 5.13: *Upper limit of Morfac for a stable model,* $\Delta x = 10m, \Delta t = 6s$

5.2.7 Comparison of numerical and analytical model

In the analytical model, there are only Morfac induced errors, in the numerical model, the model properties (grid size and time step) induce numerical errors. In the Delft3D model, not only exists the Morfac errors and numerical errors but also other errors, like the boundary algorithm and non-linear effects etc. In Delft3D model, a velocity of 1.25m/s combined with a Morfac of 1024 causes instability of the model. If the velocity, grid size and time step are all transferred into dimensionless parameters, in the numerical and analytical model, there won't be a stability problem. See Figure (5.13). The Delft3D model is the most unstable model for high Morfac maybe caused by the downwind bed level scheme, non-uniformities or other non-linear effects.

For the limited numbers of Morfac values tested in the Delft3D model, it is hard to derive an accuracy criteria. But we still can compare the errors observed in the Delft3D model results with the numerical model. From Table (5.7), Delft3D model will have more errors than the numerical model.

Table 5.7: *Accuracy analysis comparison of Delft3D model and numerical model on bed amplitude error after one wavelength*

ψ	MF	Error (Delft3D)	Error (Numerical)
8×10^{-5}	8	0.00003	0.00006
8×10^{-5}	128	0.0005	0.0012
8×10^{-5}	1024	0.0047	0.01

5.3 Conclusions

The small perturbation analysis belongs to a small morphological scale problem. Chézy friction coefficient is relatively small. So when flow velocity is not so large, the model fits in the small friction combined with small morphological scale case.

Most of the phenomenon from the analytical and numerical model can be reproduced in the Delft3D model. But the stability and the accuracy criterion derived from the analytical and numerical model is better than the Delft3D model because the non-transparent errors included in Delft3D. Therefore, the stability and accuracy criterion derived in the numerical model could serve as a necessary criterion for the Delft3D model.

1. Large value of $\psi \times MF$ will lead to instability of the model. The second surface wave φ_2 is the first to show instabilities. The necessary criteria to avoid the instability is $MF \times \psi \times Cr^{0.6} \leq 0.63$.

2. Morfac induces errors both on the surface and the bed. The bed wave amplitude is increased and shows a lagging phase error. Large flow velocities, time steps will have large errors while large grid size will have small errors. Flow velocity is the most dominant element to the critical Morfac, and model properties have a minor effect. If the bed level amplitude after one wavelength is focused, a Morfac satisfies $MF \times \psi \leq 10^{-3}$ will usually make more than 1% of error.

Chapter 6

Conclusions and Recommendations

6.1 Conclusions

After having investigated all the parameters to both the accuracy and stability of the model by applying Morfac, some conclusions can be drawn.

6.1.1 Sensitivity of Morfac

First, the sensitivity of dimensionless parameters are summarized:

1. Froude number: Large Froude number will induce large errors. But Froude number does not show a strong relation with the stability.

2. Courant number: Large Courant number will have large errors and induce stability problems.

3. Points per wave length: Large points per wave length will have smaller numerical damping which makes the model more unstable than small points per wave length, but also have less errors.

4. Friction parameter: The value of the friction parameter is related to λ_T, the morphological scale. Large friction is good for stability to the model but in the loss of accuracy.

5. ψ: The product of Morfac and ψ is the most dominant factor. In our findings, all the criteria is based on the value of $MF \times \psi$. Larger $MF \times \psi$ will not only has larger errors but also more instabilities.

If water depth is fixed, the dimensionless parameters can be transferred into dimensional parameters.

1. Flow velocity: Larger velocity both indicates larger Froude number and ψ. It is the forcing parameter of the model and it is the dominant element in the affection of Morfac. Large flow velocity will have more instability and induce more errors than the smaller one with the same Morfac.

2. Δt: Larger the time step, larger the Courant number is which will have larger errors and more instability.

3. Δx: Both the Courant number and points per wave length are affected by changing the grid size. In the Delft3D model, smaller grid size will have larger errors. Large grid size will have large numerical damping which reduce the instability, meanwhile the Morfac induced errors are also smaller.

6.1.2 Criteria of applying Morfac

The surface wave propagating opposite to the flow direction is the first to become unstable when large Morfac combined with high ψ. After investigating several Delft3D model, a necessary stability criteria for 1D unidirectional flow is derived:

$$MF \times \psi \times Cr^{0.6} \leq 0.63 \tag{6.1}$$

The accuracy criteria is hard to derive for the Delft3D case, but an estimation can be made from the criteria derived in the numerical model:

$$MF \times \psi \leq 10^{-3} \tag{6.2}$$

A Morfac value which satisfies Equation (6.2) will make more than 1% of amplitude error after one wavelength.

6.2 Recommendations

1. For 1D unidirectional flow case, friction term should be added to the equations to complete the numerical implementation of the shallow water equations. Moreover, in the Delft3D model, a large morphological scale case should be studied to prove the effect of morphological scale and friction effect in Delft3D model.

2. The effect of boundary conditions, time dependent flow and non-uniformity of the variables should be studied.

3. Other sediment transport formula should be studied to include suspended load into the analysis.

4. 2D or even 3D model should be investigated to test the effect of Morfac in more complex situations.

5. If possible, a more decent numerical implementation should be designed.

Appendix A

Mathematical operation of numerical implementation

This is the detailed linearization and dimensionless for the numerical implementation of the shallow water equations. Continued from Section (4.3.1), and the upwind scheme for bed level is used:
Stage 1:

$$S_t((U_0+U')^{p+\frac{1}{2}}) + ((U_0+U')^p)S_{1x}((U_0+U')^p) + gS_{0x}((\zeta_0+\zeta')^{p+\frac{1}{2}}) = 0$$
$$S_t((\zeta_0+\zeta')^{p+\frac{1}{2}}) + S_{0x}((h_0+h')^{p+\frac{1}{2}}(U_0+U')^{p+\frac{1}{2}}) = 0$$
$$S_t((z_{b,0}+z_b')^{p+\frac{1}{2}}) + MF \times f_U S_{0x}((U_0+U')^p) = 0$$

Stage 2:

$$S_t((U_0+U')^{p+1}) + ((U_0+U')^{p+1})S_{+x}((U_0+U')^{p+1}) + gS_{0x}((\zeta_0+\zeta')^{p+\frac{1}{2}}) = 0$$
$$S_t((\zeta_0+\zeta')^{p+1}) + S_{0x}((h_0+h')^{p+\frac{1}{2}}(U_0+U')^{p+\frac{1}{2}}) = 0$$
$$S_t((z_{b,0}+z')^{p+1}) + MF \times f_U S_{0x}((U_0+U')^{p+\frac{1}{2}}) = 0$$

After applying the equilibrium solutions, this yields:

Stage 1:

$$S_t(U'^{p+\frac{1}{2}}) + U_0 S_{1x}(U'^p) + gS_{0x}(\zeta'^{p+\frac{1}{2}}) = 0$$
$$S_t((\zeta'^{p+\frac{1}{2}}) + h_0 S_{0x}(U'^{p+\frac{1}{2}}) + U_0 S_{0x}(h'^{p+\frac{1}{2}}) = 0$$
$$S_t(z_b'^{p+\frac{1}{2}}) + MF \times f_U(U_0) S_{0x}(U'^p) = 0$$

Stage 2:

$$S_t(U'^{p+1}) + U_0 S_{+x}(U'^{p+1}) + gS_{0x}(\zeta'^{p+\frac{1}{2}}) = 0$$
$$S_t(\zeta'^{p+1}) + U_0 S_{0x}(h')^{p+\frac{1}{2}} + h_0 S_{0x}(U'^{p+\frac{1}{2}}) = 0$$
$$S_t(z_b'^{p+1}) + MF \times f_U(U_0) S_{0x}(U'^{p+\frac{1}{2}}) = 0$$

If the solutions are assumed to have a form like:

$$\begin{pmatrix} U_m^{p\,\prime} \\ h_m^{p\,\prime} \\ z_{b,m}^{p\quad\prime} \end{pmatrix} = \begin{pmatrix} \hat{U^p}' \\ \hat{h^p}' \\ \hat{z_b^p}' \end{pmatrix} e^{imk\Delta x}$$

It leads to:

Stage 1:

Momentum equation:

$$S_t(U'^{p+\frac{1}{2}}) + U_0 S_{1x}(U'^p) + gS_{0x}(\zeta'^{p+\frac{1}{2}}) = 0$$
$$\frac{U'^{p+\frac{1}{2}}_{\quad m+\frac{1}{2}} - U'^{p}_{\quad m+\frac{1}{2}}}{\frac{1}{2}\Delta t} + U_0 \frac{U'^{p}_{\quad m+\frac{3}{2}} - U'^{p}_{\quad m-\frac{1}{2}}}{2\Delta x} + g\frac{\zeta'^{p+\frac{1}{2}}_{\quad m+1} - \zeta'^{p+\frac{1}{2}}_{\quad m}}{\Delta x} = 0$$
$$\frac{\hat{U'}^{p+\frac{1}{2}} - \hat{U'}^{p}}{\frac{1}{2}\Delta t} e^{ik(m+\frac{1}{2})\Delta x} + U_0 \frac{\hat{U'}^{p}(1 - e^{-ik\Delta x})}{2\Delta x} e^{ik(m+\frac{1}{2})\Delta x}$$
$$+ g\frac{\hat{\zeta'}^{p+\frac{1}{2}}(1 - e^{-ik\frac{1}{2}\Delta x})}{\Delta x} e^{ik(m+\frac{1}{2})\Delta x} = 0$$
$$\hat{U'}^{p+\frac{1}{2}} + \frac{g\Delta t i \sin\frac{1}{2}k\Delta x}{\Delta x}\hat{\zeta'}^{p+\frac{1}{2}} = (1 - \frac{U_0\Delta t i(\sin k\Delta x)}{2\Delta x})\hat{U'}^{p}$$

Continuity equation:

$$S_t((\zeta'^{p+\frac{1}{2}}) + h_0 S_{0x}(U'^{p+\frac{1}{2}}) + U_0 S_{0x}(h'^{p+\frac{1}{2}}) = 0$$

$$\frac{\zeta'^{p+\frac{1}{2}}_m - \zeta'^{p}_m}{\frac{1}{2}\Delta t} + (\zeta_0 - z_{b,0})\frac{U'^{p+\frac{1}{2}}_{m+\frac{1}{2}} - U'^{p+\frac{1}{2}}_{m-\frac{1}{2}}}{\Delta x} + U_0\frac{\zeta'^{p+\frac{1}{2}}_m - \zeta'^{p+\frac{1}{2}}_{m-1}}{\Delta x} - U_0\frac{z_b'^{\,p+\frac{1}{2}}_m - z_b'^{\,p+\frac{1}{2}}_{m-1}}{\Delta x} = 0$$

$$\frac{\hat{\zeta}'^{p+\frac{1}{2}} - \hat{\zeta}'^{p}}{\frac{1}{2}\Delta t}e^{ikm\Delta x} + (\zeta_0 - z_{b,0})\frac{\hat{U}'^{p+\frac{1}{2}}(e^{ik\frac{1}{2}\Delta x} - e^{-ik\frac{1}{2}\Delta x})}{\Delta x}e^{ikm\Delta x}$$

$$+U_0\frac{(\hat{\zeta}'^{p+\frac{1}{2}} - \hat{z}_b'^{p+\frac{1}{2}})(1 - e^{-ik\Delta x})}{\Delta x}e^{ikm\Delta x}$$

$$\frac{(\zeta_0 - z_{b,0})\Delta t i \sin\frac{1}{2}k\Delta x}{\Delta x}\hat{U}'^{p+\frac{1}{2}} + (1 + \frac{U_0\Delta t(1 - e^{-ik\Delta x})}{2\Delta x})\hat{\zeta}'^{p+\frac{1}{2}} - \frac{U_0\Delta t(1 - e^{-ik\Delta x})}{2\Delta x}\hat{z}_b'^{p+\frac{1}{2}} = \hat{\zeta}'^{p}$$

Morphology change:

$$S_t(z_b'^{p+\frac{1}{2}}) + MF \times f_U(U_0) S_{0x}(U'^{p+\frac{1}{2}}) = 0$$

$$\frac{z'^{p+\frac{1}{2}}_{b,m} - z'^{p}_{b,m}}{\frac{1}{2}\Delta\tau} + MF \times f_U(U_0)\frac{U'^{p+\frac{1}{2}}_{m+\frac{1}{2}} - U'^{p+\frac{1}{2}}_{m-\frac{1}{2}}}{\Delta x} = 0$$

$$\frac{\hat{z}_b'^{p+\frac{1}{2}} - \hat{z}_b'^{p}}{\frac{1}{2}\Delta\tau}e^{ikm\Delta x} + MF \times f_U(U_0)\frac{\hat{U}'^{p+\frac{1}{2}}(e^{ik\frac{1}{2}\Delta x} - e^{-ik\frac{1}{2}\Delta x})}{\Delta x}e^{ikm\Delta x} = 0$$

$$\hat{z}_b'^{p+\frac{1}{2}} = -\frac{MF \times f_U(U_0)\Delta t i(\sin\frac{1}{2}k\Delta x + \sin\frac{3}{2}k\Delta x)}{4\Delta x}\hat{U}'^{p} + \hat{z}_b'^{p}$$

The same for the stage 2. So the linearized equations are:

Stage 1:

$$\hat{U}'^{p+\frac{1}{2}} + \frac{g\Delta t i \sin\frac{1}{2}k\Delta x}{\Delta x}\hat{\zeta}'^{p+\frac{1}{2}} = (1 - \frac{U_0\Delta t i \sin k\Delta x}{2\Delta x})\hat{U}'^{p}$$

$$\frac{(\zeta_0 - z_{b,0})\Delta t i \sin\frac{1}{2}k\Delta x}{\Delta x}\hat{U}'^{p+\frac{1}{2}} + (1 + \frac{U_0\Delta t(1 - e^{-ik\Delta x})}{2\Delta x})\hat{\zeta}'^{p+\frac{1}{2}}$$

$$-\frac{U_0\Delta t(1 - e^{-ik\Delta x})}{2\Delta x}\hat{z}_b'^{p+\frac{1}{2}} = \hat{\zeta}'^{p}$$

$$\hat{z}_b'^{p+\frac{1}{2}} = \frac{MF \times f_U(U_0)\Delta t i(\sin\frac{1}{2}k\Delta x + \sin\frac{3}{2}k\Delta x)}{4\Delta x}\hat{U}'^{p} + \hat{z}_b'^{p}$$

Stage 2:

$$(1+\frac{U_0\Delta t\text{sign}(U)(3-4e^{-ik\Delta x}+e^{-2ik\Delta x})}{4\Delta x})\hat{U}'^{p+1}=\hat{U}'^{p+\frac{1}{2}}-\frac{g\Delta\tau i\sin\frac{1}{2}k\Delta x}{\Delta x}\hat{\zeta}'^{p+\frac{1}{2}}$$
$$\hat{\zeta}'^{p+1}=-\frac{(\zeta_0-z_{b,0})\Delta ti\sin\frac{1}{2}k\Delta x}{\Delta x}\hat{U}'^{p+\frac{1}{2}}+(1-\frac{U_0\Delta t(1-e^{-ik\Delta x})}{2\Delta x})\hat{\zeta}'^{p+\frac{1}{2}}$$
$$+\frac{U_0\Delta t(1-e^{-ik\Delta x})}{2\Delta x}\hat{z}_b'^{p+\frac{1}{2}}$$
$$\hat{z}_b'^{p+1}=-\frac{MF\times f_U(U_0)\Delta ti(\sin\frac{1}{2}k\Delta x+\sin\frac{3}{2}k\Delta x)}{4\Delta x}\hat{U}'^{p+\frac{1}{2}}+\hat{z}_b'^{p+\frac{1}{2}}$$

Further dimensionless is done by introducing:

$$U'=c_TU_D,$$
$$\zeta'=h_Th_D,$$
$$z_b'=h_Tz_{b,D}$$

Stage 1:

$$\hat{U}_D'^{p+\frac{1}{2}}+\frac{gh_T}{c_T}\frac{\Delta ti\sin\frac{1}{2}k\Delta x}{\Delta x}\hat{\zeta}_D'^{p+\frac{1}{2}}=(1-\frac{U_0\Delta ti\sin k\Delta x}{2\Delta x})\hat{U}_D'^{p}$$
$$\frac{(\zeta_0-z_{b,0})}{h_T}\frac{c_T\Delta ti\sin\frac{1}{2}k\Delta x}{\Delta x}\hat{U}_D'^{p+\frac{1}{2}}+(1+\frac{U_0\Delta t(1-e^{-ik\Delta x})}{2\Delta x})\hat{\zeta}_D'^{p+\frac{1}{2}}$$
$$-\frac{U_0\Delta t(1-e^{-ik\Delta x})}{2\Delta x}\hat{z}_b'^{p+\frac{1}{2}}=\hat{\zeta}_D'^{p}$$
$$\hat{z}_D'^{p+\frac{1}{2}}=-MF\times\frac{f_U(U_0)}{h_T}\frac{c_T\Delta ti(\sin\frac{1}{2}k\Delta x+\sin\frac{3}{2}k\Delta x)}{4\Delta x}\hat{U}_D'^{p}+\hat{z}_D'^{p}$$

Stage 2:

$$(1+\frac{U_0\Delta t\text{sign}(U)(3-4e^{-ik\Delta x}+e^{-2ik\Delta x})}{4\Delta x})\hat{U}_D'^{p+1}=\hat{U}_D'^{p+\frac{1}{2}}-\frac{gh_T\Delta ti\sin\frac{1}{2}k\Delta x}{c_T\Delta x}\hat{\zeta}_D'^{p+\frac{1}{2}}$$
$$\hat{\zeta}_D'^{p+1}=-\frac{\zeta_0-z_{b,0}}{h_T}\frac{c_T\Delta ti\sin\frac{1}{2}k\Delta x}{\Delta x}\hat{U}_D'^{p+\frac{1}{2}}+(1-\frac{U_0\Delta t(1-e^{-ik\Delta x})}{2\Delta x})\hat{\zeta}_D'^{p+\frac{1}{2}}$$
$$+\frac{U_0\Delta t(1-e^{-ik\Delta x})}{2\Delta x}\hat{z}_{b,D}'^{p+\frac{1}{2}}$$
$$\hat{z}_{b,D}'^{p+1}=-MF\times\frac{f_U(U_0)}{h_T}\frac{c_T\Delta ti(\sin\frac{1}{2}k\Delta x+\sin\frac{3}{2}k\Delta x)}{4\Delta x}\hat{U}_D'^{p+\frac{1}{2}}+\hat{z}_{b,D}'^{p+\frac{1}{2}}$$

The final dimensionless equations are:

Stage 1:

$$\hat{U'_D}^{p+\frac{1}{2}} + Cr \times i \sin\frac{1}{2}n\hat{\zeta'_D}^{p+\frac{1}{2}} = (1 - Cr \times Fr \times \frac{i\sin n}{2})\hat{U'_D}^{p}$$

$$Cri \sin\frac{1}{2}n\hat{U'_D}^{p+\frac{1}{2}} + (1 + Cr \times Fr \times \frac{1 - e^{-in}}{2})\hat{\zeta'_D}^{p+\frac{1}{2}} - Cr \times Fr \times \frac{1 - e^{-in}}{2}\hat{z'_D}^{p+\frac{1}{2}} = \hat{\zeta'_D}^{p}$$

$$\hat{z'_D}^{p+\frac{1}{2}} = \hat{z'_D}^{p} - \frac{1}{4}MF \times Cr \times \psi \times i(\sin\frac{1}{2}n + \sin\frac{3}{2}n)\hat{U'_D}^{p+\frac{1}{2}}$$

Stage 2:

$$(1 + \frac{Fr \times Cr \times (3 - 4e^{-in} + e^{-2in})}{4})\hat{U'_D}^{p+1} = \hat{U'_D}^{p+\frac{1}{2}} - Cri \sin\frac{1}{2}n\hat{\zeta'_D}^{p+\frac{1}{2}}$$

$$\hat{\zeta'_D}^{p+1} = -Cr \times i \sin\frac{1}{2}n\hat{U'_D}^{p+\frac{1}{2}} + (1 - Fr \times Cr \times \frac{1 - e^{-in}}{2})\hat{\zeta'_D}^{p+\frac{1}{2}} + Fr \times Cr \times \frac{1 - e^{-in}}{2}\hat{z'_{b,D}}^{p+\frac{1}{2}}$$

$$\hat{z'_{b,D}}^{p+1} = \hat{z'_{b,D}}^{p+\frac{1}{2}} - \frac{1}{4}MF \times Cr \times \psi \times i(\sin\frac{1}{2}n + \sin\frac{3}{2}n)\hat{U'_D}^{p+1}$$

Bibliography

[1] C.M.Swinkels. Memo: Status Morfac Research. *Deltares Memo*, 2009.

[2] P.J. Cowell and B.G. Thom. Morphodynamics of coastal evolution. *Coastal evolution: Late Quaternary shoreline morphodynamics*, pages 33–86, 1994.

[3] H.J. De Vriend. Mathematical modelling and large-scale coastal behaviour. *Journal of Hydraulic Research*, 29(6):727–740, 1991.

[4] H.J. De Vriend, M. Capobianco, T. Chesher, H.E. De Swart, B. Latteux, and M.J.F. Stive. Approaches to long-term modelling of coastal morphology: a review. *Coastal Engineering*, 21(1-3):225–269, 1993.

[5] N.M. Grunnet, D.J.R. Walstra, and B.G. Ruessink. Process-based modelling of a shoreface nourishment. *Coastal engineering*, 51(7):581–607, 2004.

[6] G. LESSER. An approach to medium-term coastal morphological modelling: phd (paperback). 2009.

[7] G.R. Lesser, J.A. Roelvink, J. Van Kester, and G.S. Stelling. Development and validation of a three-dimensional morphological model. *Coastal Engineering*, 51(8-9):883–915, 2004.

[8] A. Reniers, J.A. Roelvink, and E.B. Thornton. Morphodynamic modeling of an embayed beach under wave group forcing. *Journal of Geophysical research*, 109(C1):C01030, 2004.

[9] J.A. Roelvink. Coastal morphodynamic evolution techniques. *Coastal Engineering*, 53(2-3):277–287, 2006.

[10] J.G. Slootweg, J. Persson, A.M. Van Voorden, G.C. Paap, and W.L. Kling. A study of the eigenvalue analysis capabilities of power system dynamics simulation software. In *Proc. 14th Power Systems Computation Conference*.

[11] M. Van der Wegen and JA Roelvink. Long-term morphodynamic evolution of a tidal embayment using a two-dimensional, process-based model. *J. Geophys. Res*, 113, 2008.

[12] Z.B. Wang, T. Louters, and H.J. De Vriend. Morphodynamic modelling for a tidal inlet in the Wadden Sea. *Marine geology*, 126(1-4):289–300, 1995.